ANNUAL REVIEWS

Annual Review of Earth and Planetary Sciences

Titan's Interior Structure and Dynamics After the Cassini-Huygens Mission

Christophe Sotin,[1,2] Klára Kalousová,[3] and Gabriel Tobie[4]

[1]Jet Propulsion Laboratory, California Institute of Technology, Pasadena, California 91109, USA

[2]Current affiliation: Laboratoire de Planétologie et Géodynamique, CNRS UMR 6112, Université de Nantes, 44322 Nantes, France; email: Christophe.Sotin@univ-nantes.fr

[3]Department of Geophysics, Faculty of Mathematics and Physics, Charles University, 180 00 Praha 8, Czech Republic

[4]Laboratoire de Planétologie et Géodynamique, CNRS UMR 6112, Université de Nantes, 44322 Nantes, France

Annu. Rev. Earth Planet. Sci. 2021. 49:579–607

First published as a Review in Advance on March 22, 2021

The *Annual Review of Earth and Planetary Sciences* is online at earth.annualreviews.org

https://doi.org/10.1146/annurev-earth-072920-052847

Keywords

Titan, planetary interior, planetary evolution, ocean worlds, Cassini-Huygens mission

Abstract

The Cassini-Huygens mission that explored the Saturn system during the period 2004–2017 revolutionized our understanding of Titan, the only known moon with a dense atmosphere and the only body, besides Earth, with stable surface liquids. Its predominantly nitrogen atmosphere also contains a few percent of methane that is photolyzed on short geological timescales to form ethane and more complex organic molecules. The presence of a significant amount of methane and ^{40}Ar, the decay product of ^{40}K, argues for exchange processes from the interior to the surface. Here we review the information that constrains Titan's interior structure. Gravity and orbital data suggest that Titan is an ocean world, which implies differentiation into a hydrosphere and a rocky core. The mass and gravity data complemented by equations of state constrain the ocean density and composition as well as the hydrosphere thickness. We present end-member models, review the dynamics of each layer, and discuss the global evolution consistent with the Cassini-Huygens data.

- Titan is the only moon with a dense atmosphere where organic molecules are synthesized and have sedimented at the surface.

- The Cassini-Huygens mission demonstrated that Titan is an ocean world with an internal water shell and liquid hydrocarbon seas at the poles.
- Interactions between water, rock, and organics may have occurred during most of Titan's evolution, which has strong astrobiological implications.
- Data collected by the Dragonfly mission and comparison with the JUpiter ICy moons Explorer (JUICE) data for Ganymede will further reveal Titan's astrobiology potential.

1. INTRODUCTION

Titan is the second largest satellite in the Solar System after Jupiter's moon Ganymede. It is the only icy moon with a dense atmosphere made of mostly nitrogen (∼98 wt%) and methane (<2 wt%) (Bézard 2014). The methane abundance varies significantly throughout the atmosphere, from 1.5% in the stratosphere to more than 5% in the troposphere (Niemann et al. 2010, Bézard 2014). The surface conditions, pressure of 0.15 MPa and temperature of 94 K, are such that methane and ethane (produced by photolysis of methane) are liquid and form lakes and seas mostly located at the north pole (Stofan et al. 2007). But methane is irreversibly photolyzed in the upper atmosphere, and the present amount would disappear in a few tens of millions of years (e.g., Yung et al. 1984, Griffith et al. 2013), which is short on geological timescales, thus requiring an interior reservoir and a replenishment process. The presence of ^{40}Ar, a daughter element from the decay of ^{40}K, also implies exchange processes between the K reservoir, likely silicates, and the atmosphere. Finally, the observed $^{15}N/^{14}N$ isotope ratio suggests that up to 50% of the atmospheric nitrogen could come from the decomposition of insoluble organic matter (IOM) present in Titan's interior (Miller et al. 2019). Understanding the formation of Titan's atmosphere requires knowledge of its interior structure and models of its evolution constrained by observations.

The National Aeronautics and Space Administration (NASA), European Space Agency (ESA), and Italian Space Agency (ASI) Cassini-Huygens mission observed the Saturn system during the period 2004–2017 using Titan's gravity assist to explore the diversity of objects and make in situ measurements at different locations. Determining the interior structure of a planet or satellite from orbit is best achieved by measuring the gravity and magnetic fields. On January 14, 2005, the ESA Huygens probe plunged into Titan's atmosphere and provided the first detailed information on Titan's atmosphere (Fulchignoni et al. 2005, Niemann et al. 2005) and close-up views of Titan's surface (Tomasko et al. 2005). During 13 years, the NASA Cassini spacecraft performed 127 close Titan flybys including 9 dedicated to the determination of the gravity field (Iess et al. 2010, 2012; Durante et al. 2019). One important result has been the determination of the tidal Love number k_2, whose large value implies the presence of a deep ocean (Iess et al. 2012). In addition to being the only moon with a dense atmosphere and the only object in the Solar System, besides Earth, with liquids at its surface, Titan is also an ocean world (**Figure 1**). The gravity measurements also provided values of the moment of inertia (MoI) that is an integrated value of the density distribution, suggesting that Titan is differentiated into a hydrosphere and an inner rocky core (Castillo-Rogez & Lunine 2010). After summarizing the different observations (Section 2), this review describes the interior structure models that are consistent with these observations and use the most recent equations of state (EoS) (Section 3). Section 4 discusses the thermal evolution models and is followed by a discussion of the hydrosphere dynamics and implications for atmosphere recycling (Section 5).

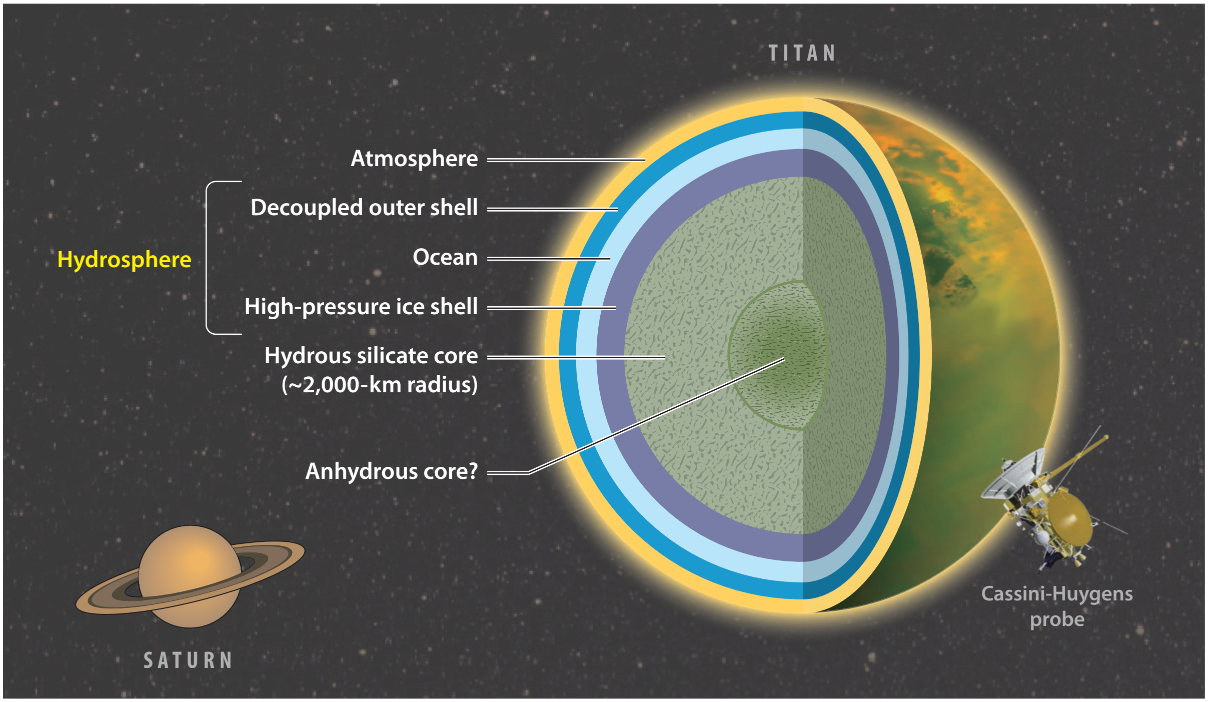

Figure 1

Titan's interior structure. The rocky core is likely composed of hydrated silicates to account for the high value of the moment of inertia. It is overlaid by a hydrosphere that includes a deep salty ocean.

2. OBSERVATIONS

The Cassini-Huygens mission aimed to answer two science questions related to Titan's interior structure: (*a*) Is there a deep ocean? and (*b*) How much is Titan differentiated? As proven by previous missions, determining the gravity field, in particular the degree 2 coefficients, provides answers to these questions. Additional constraints come from the shape, the electromagnetic field, the surface morphological features and composition, and the orbital and rotational characteristics.

2.1. Gravity Coefficients

The gravity field provides information on the mass distribution inside Titan. The gravity coefficients are determined by monitoring the line of sight velocity change of the Cassini spacecraft as it flies by Titan. The closer to the moon, the more precise the determination of the gravity field. However, Titan has an extended atmosphere, and the drag would add a large contribution to the spacecraft velocity. An optimum closest approach flyby altitude of 1,500 km was a compromise between the atmospheric perturbations and precision. After the first four flybys, Iess et al. (2010) were able to retrieve the gravity coefficients up to degree 3. The degree 2 gravity coefficients, J_2 and C_{22} (**Table 1**), include a constant component and a periodic component that is proportional to the eccentricity and therefore less than a few percent of the constant component. Because Titan is in a spin-orbit resonance, it has an ellipsoidal shape that leads to a high value of the C_{22} coefficient. If Titan is in a hydrostatic equilibrium, the degree 2 coefficients are related by a simple relation:

Table 1 Parameters for Titan

Parameter	Measurement
Semimajor axis to Saturn (km)	1.2218×10^6
Eccentricity (%)	2.846
Synchronous sidereal rotational period (s)	1,377,684 ~ 15.945 Earth days
GM (km^3/s^2)	8,978.1383 (3)
Mass (10^{22} kg)/density (kg/m^3)	13.4522 (3)/1,881.46 (11)
Mean radius (R) (km)	2,574.765 (18)
Shape triaxial ellipsoid (a, b, c) (km)	2,575.124 (26), 2,574.746 (45), 2,574.414 (28)
Degree 2 gravity coefficients: J_2 and C_{22} ($\times 10^6$)	33.1 (6), 10.38 (8)
Reduced moment of inertia C/MR^2	0.341
Tidal Love number k_2	0.616 (67)
$q = \omega^2 R^3/GM$	3.96×10^{-5}
Gravity acceleration (m/s^2) at the surface	1.3543
Estimated radiogenic power (GW)	300–400
Obliquity (°)	0.305 (3)

The numbers in parentheses indicate the uncertainty on the last digits when the information is available. Abbreviation: *GM*, gravitational parameter. GM, J_2, C_{22}, and k_2 from Durante et al. (2019); shape parameters from Corlies et al. (2017); estimated power from Chen et al. (2014); obliquity value from Meriggiola et al. (2016).

$J_2 = 10/3\ C_{22}$. The retrieved values (**Table 1**) give a ratio of 3.19, which is 1.7 standard deviation from the theoretical value of 10/3, suggesting a slight departure from hydrostatic equilibrium (Durante et al. 2019) (see Section 3.1 for the implications on the interior structure). With the nine dedicated flybys, Durante et al. (2019) were able to obtain the gravity field up to degree 5.

It was critical to measure the degree 2 tidal Love number (see the sidebar titled Love Number) because it puts a strong constraint on the presence of an ocean. This was made possible by having dedicated gravity flybys performed when Titan was near its orbit pericenter and apocenter, maximizing gravity changes (Iess et al. 2012). The value of k_2 depends on several parameters including the ocean density, the ice shell thickness, and the heat transfer mechanism through the ice shell

LOVE NUMBER

The measurement of the gravity field provides information on Titan's interior structure. The degree 2 coefficients have a static component (coefficients J_2 and C_{22}) and a time-dependent part due to Titan's synchronous eccentric orbit around Saturn. The static components J_2 and C_{22} are a measure of the polar flattening and the equatorial ellipticity, respectively. Their values are linked to the three moments of inertia relative to the axis of Titan's ellipsoid shape. The moments of inertia are determined by the density distribution in Titan's interior. For an interior structure not too far from hydrostatic equilibrium, the knowledge of the static coefficients provides constraints on the average density profile. The eccentricity causes a time variation of the degree 2 tidal potential, resulting in a time-dependent degree 2 tidal deformation of Titan's surface and interior. As a consequence, the polar flattening and the equatorial ellipticity vary with time, which modulates the degree 2 coefficients of the gravity field. The time variations of the degree 2 coefficients are proportional to the tidal Love number, which is a measure, outside the deformed body, of the gravitational potential induced by time-varying internal mass redistribution due to tidal forcing. It corresponds to the ratio between the internal potential induced by mass redistribution and the external perturbing potential raised by Saturn's gravity.

(Mitri et al. 2014). It also depends on the presence of ocean waves that can be triggered if the ocean is stratified. If the ocean is made of pure water, the value of k_2 is around 0.5 (Mitri et al. 2014). Durante et al. (2019) report a value of 0.616, about 1.7 standard deviation larger than the value of 0.5 for pure water. This large value can be explained by either a higher density due to the presence of salts, waves in a stratified ocean, or a combination of the two.

2.2. Shape and Topography

Titan's shape was determined by the radar onboard the Cassini spacecraft (Elachi et al. 2004). Three data sets are available (Corlies et al. 2017). First, the Synthetic Aperture Radar (SAR) topography covers ~5.2% of Titan's surface with an average error in elevation of ~160 m over all 122 profiles. Second, the radar in its altimeter mode mapped ~1.6% of Titan's surface along 69 profiles. Although altimetry provides a much smaller coverage compared to SAR topography, the vertical error is only ~35 m (Zebker et al. 2009). Finally, 19 digital terrain models (DTMs) were constructed through stereophotogrammetry. They cover an additional ~2.1% of Titan's surface, with a typical error of ~100 m (Kirk et al. 2013). These three data sets provide an incomplete coverage of Titan's surface. However, it was possible to retrieve Titan's shape—i.e., the difference between the surface and a sphere radius of 2,575 km—up to a degree 8. The shape is characterized by polar depressions up to 800 m deep. The topography (**Figure 2*a***) is the difference between Titan's shape and an equipotential surface, which is mainly dominated by the first two degrees of the gravity field. Titan is characterized by small topography variations at large wavelengths, from about −600 m for the south polar depression to +400 m for some midlatitude highlands. The polar dynamical flattening can explain only half of the polar depressions observed in the shape model. If these depressions were not isostatically compensated, the J_2/C_{22} ratio would be much larger than the observed value because J_2 strongly depends on uncompensated polar topography (Gao & Stevenson 2013), whereas C_{22} does not. Therefore, the depressions must be compensated for by either a different thickness of the ice shell between the pole and the equator (Airy model proposed in Nimmo & Bills 2010) or differences in density (Pratt model proposed in Choukroun & Sotin 2012). These two models are discussed in Section 5.3 and are linked to different physical processes that may operate at Titan—differences in the heat flux transported through the ocean for the Airy model (Section 5.2) and formation of a dense ethane clathrate layer at the poles for the Pratt model.

The depressions at the north pole are consistent with the presence of hydrocarbon seas, such as Kraken Mare, that were first observed by the radar instruments (Stofan et al. 2007). A large region named Xanadu centered at 15°S, 120°W and extending from 60°W to 150°W also correlates with a depression (**Figure 2**). Other equatorial topographic variations do not seem to correlate with geological features that are dominated by dune fields [Visual and Infrared Mapping Spectrometer (VIMS)/Imaging Science Subsystem map, **Figure 2*b***]. As pointed out by Corlies et al. (2017), the absence of dune fields in the Xanadu region is not explained, as the sand would likely be transported to low topography. It suggests that Xanadu may be a very recent feature.

2.3. Rotational and Orbital Characteristics

Titan's rotation can provide additional constraints on the internal structure. Neglecting polar motion, the rotational state of a synchronous satellite can be considered as consisting of two components: the rotation rate variations with respect to the expected synchronous rotation rate—i.e., the nonsynchronous rotation (NSR) rate—and the obliquity, corresponding to the

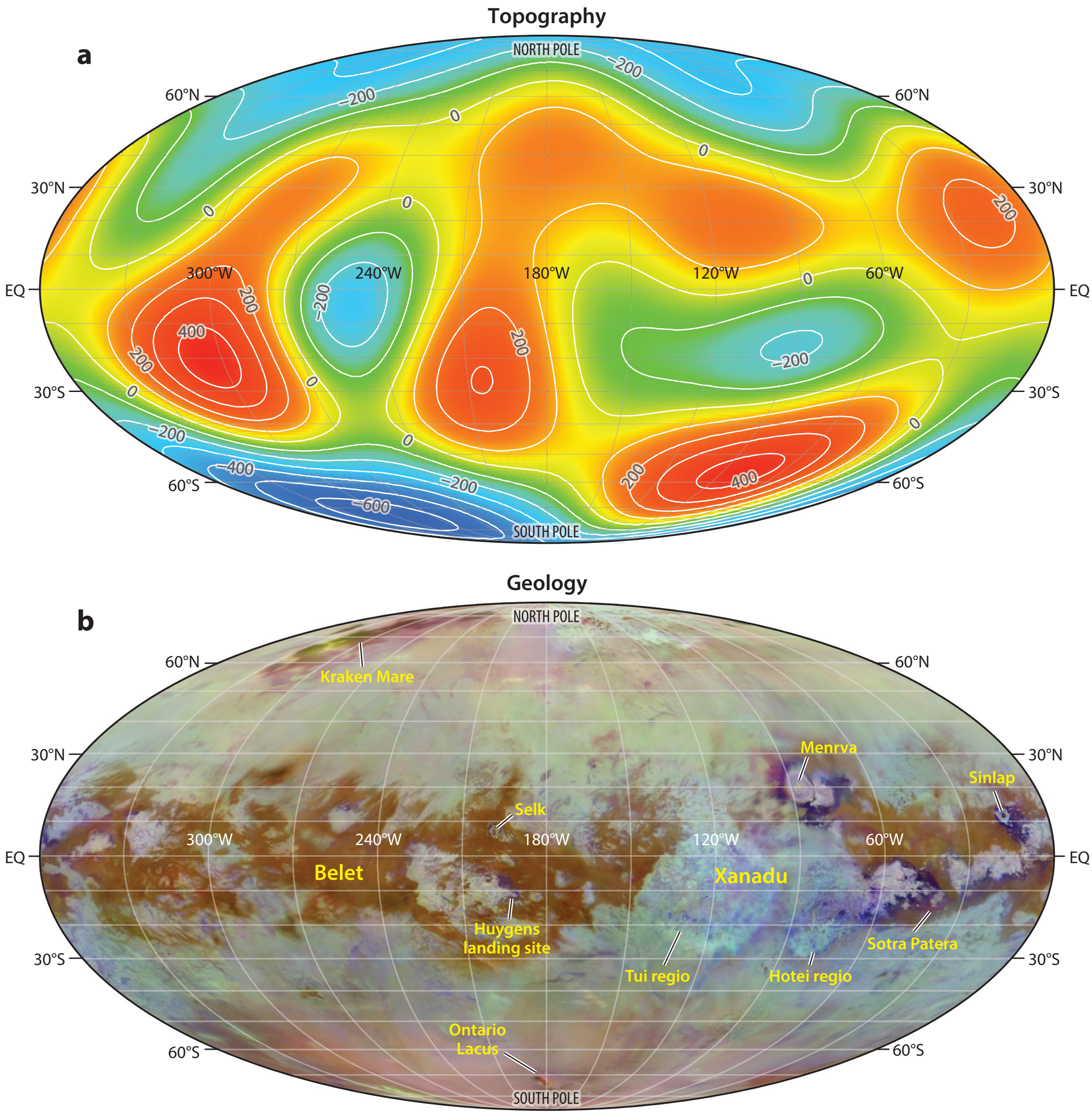

Figure 2

Mollweide projections centered at 180° show (*a*) Titan's topography and (*b*) a Visual and Infrared Mapping Spectrometer/Imaging Science Subsystem color map with the different geological regions (Le Mouélic et al. 2019). In panel *a*, contours are in meters. The topography is calculated from coefficients in Corlies et al. (2017), truncated to degree 5. The equipotential surface is determined from gravity coefficients in Durante et al. (2019).

angle between the rotation axis and the axis normal to the orbital plane (e.g., Baland et al. 2014). The value of the NSR rate has been updated several times since its first estimation of 0.36°/year by Lorenz et al. (2008) from radar surface images (see also Stiles et al. 2008). Lorenz et al. (2008) have interpreted this high NSR rate as evidence of a subsurface ocean, allowing a decoupling between the deep interior and the ice shell forced by the atmospheric torque. Subsequent data reprocessing by Stiles et al. (2008) indicated a smaller NSR rate (0.11°/year). Using two additional years of data, Meriggiola & Iess (2012) found a very small NSR rate compatible with synchronous rotation (±0.02°/year). By modeling the gravitational and pressure coupling between the shell and the interior, Van Hoolst et al. (2009, 2013) predicted a maximal NSR rate of about 0.013°/year, smaller than the last available estimation of Meriggiola & Iess (2012), which excludes the possibility to retrieve useful constraints on the interior structure.

The obliquity of Titan is estimated to be about 0.3° (Stiles et al. 2008, Meriggiola et al. 2016), which is about three times larger than 0.12°—the value expected for an entirely solid Titan (Bills & Nimmo 2008). This high value has been interpreted as being indicative of the presence of an internal ocean (Bills & Nimmo 2008, 2011; Baland et al. 2011, 2014). By computing the obliquity from a Cassini state model for a differentiated interior structure with each layer having an ellipsoidal shape consistent with the measured surface shape and gravity field, Baland et al. (2014) showed that the observed obliquity implies a relatively dense and deep ocean. However, as a wide range of internal models can explain the observed value, no firm conclusion about the interior structure can be drawn from the obliquity alone.

Another important constraint on the interior of Titan and its past evolution is provided by the orbital characteristics. Titan exhibits an orbital eccentricity (3%) several times higher than its Jovian cousins Europa, Io, and Ganymede. Contrary to the Jovian moons, no orbital resonance in the Saturnian system is able to force Titan's eccentricity, and thus the frictional damping due to tides raised by Saturn should lead to progressive circularization of Titan's eccentric orbit. The high eccentricity has been classically interpreted as evidence of reduced dissipation on Titan, implying limited surface liquid bodies (Sagan & Dermott 1982, Sears 1995) and no liquid water ocean at depth (Sohl et al. 1995). Using a coupled thermal-orbital model, Tobie et al. (2005a, 2006) showed that the current eccentricity may be compatible with the presence of an internal ocean but would imply a larger eccentricity in the past and an ocean beneath a relatively thin and weakly dissipative ice shell during most of Titan's evolution. The proximity of small Hyperion suggests that the past eccentricity probably never exceeded 0.1–0.2. However, the 4:3 orbital resonance between Hyperion and Titan remains problematic. Recently, using very accurate radio tracking of the Cassini spacecraft during multiple flybys, Lainey et al. (2020) measured Titan's orbital expansion rate. They showed that Titan is migrating outward much faster than initially anticipated, owing to a strong dissipation inside Saturn. This finding implies that Titan formed much closer to Saturn and has migrated outward to its current position. Consequently, Titan experienced much stronger tidal forcing in the past, which may have major implications for its past internal activity.

2.4. Atmosphere and Surface Constraints

The atmosphere composition depends on several processes including endogenic processes that lead to outgassing. One major enigma of Titan's global dynamics is the need for methane replenishment against its upper atmosphere photolysis—the present amount of atmospheric methane would be photolyzed in a few tens of millions of years, which is short on geological timescales (Yung et al. 1984). In the absence of a global surface ocean, the methane reservoir must be in the subsurface where it can be destabilized by internal processes (e.g., Tobie et al. 2006, Choukroun et al. 2010) or by impacts (Choukroun & Sotin 2012, Zahnle et al. 2014). A large amount of ^{40}Ar [mole fraction of 3.39 (±0.12) $\times 10^{-5}$] was measured in Titan's atmosphere by the gas chromatograph mass spectrometer onboard the Huygens probe (Niemann et al. 2010). This corresponds to a total mass of 4.5 (±0.2) $\times 10^{14}$ kg. Because ^{40}Ar is a product of the radioactive decay of ^{40}K, its presence in the atmosphere indicates its release from the silicates, which represent the most likely initial reservoir of ^{40}K. Depending on assumptions on the K/Si ratio in the silicates that compose Titan's rocky core (i.e., the type of chondritic material), the amount of atmospheric ^{40}Ar represents between 10% and 20% of the potential ^{40}Ar. The remaining ^{40}Ar could still be present in the rocky core or dissolved in the ocean or the hydrocarbon seas (e.g., Tobie et al. 2012). Finally, a recent study by Miller et al. (2019) suggests that up to 50% of Titan's nitrogen comes from the decomposition of IOM contained in Titan's rocky core when it warms up. The amount of outgassed nitrogen is inferred from dual considerations of the $^{15}N/^{14}N$ isotope ratio (167.7 ± 0.6) and the $^{36}Ar/N$ ratio in Titan's atmosphere from Niemann et al. (2010). All the above points demonstrate that exchange processes between the interior and the surface have existed during Titan's geological history, although the timings of these outgassing events are not well constrained. Models of Titan's evolution should account for these results.

Another characteristic of Titan is the paucity of impact craters with only about 60 features that rank from certain (12) including Selk, Sinlap, and Menrva (**Figure 2*b***) to nearly certain (25) to probable (25) (Werynski et al. 2019). The density of impact craters is a proxy for determining the age of a planetary surface. The scarcity of impact craters favors a young age for Titan's surface, between 0.2 and 1 Gyr (Neish & Lorenz 2012). In addition, the presence of impact craters provides information on the thickness of Titan's lithosphere. The size of Titan's largest impact crater, Menrva (diameter of 425 km) (**Figure 2**), suggests a lithosphere at least some tens of kilometers thick at the time of formation.

Finally, the surface composition can provide information about a potential resurfacing. Titan's surface is covered with organic aerosol forming in its upper atmosphere by the photolysis of methane and further reactions with nitrogen (e.g., Hörst 2017). All of Titan's surface should be coated with these aerosols that eventually turn into sand to form the dune fields. However, some areas appear different in false-color infrared images of Titan's surface (**Figure 2*b***)—the dark blue color is interpreted as regions enriched in water ice (Griffith et al. 2019, Le Mouélic et al. 2019). The origin of these terrains seems to be related to exogenic processes such as impact craters (e.g., Le Mouélic et al. 2008) and erosion (Jaumann et al. 2008, Griffith et al. 2019). Evidence for endogenic processes is limited to a potential cryovolcano in the Sotra Facula regio (Lopes et al. 2013) and tentative interpretation of flow-like features in the Tui regio and Hotei regio (Barnes et al. 2006). Confirmation that these features have a volcanic origin would require higher-resolution observations as well as composition information.

2.5. Electromagnetic Measurements

Magnetic field measurements can provide key information on the interior structure of an ocean world as demonstrated by the Galileo mission. The magnetometers on the Galileo spacecraft detected Ganymede's permanent magnetic field best interpreted by the presence of an iron-rich liquid core (Kivelson et al. 1996). They also detected inductive magnetic fields at Ganymede, Europa, and Callisto (Khurana et al. 1998, Kivelson et al. 2002), which are best interpreted by the presence of a deep, salty ocean. However, such measurements at Titan are challenged by three facts (e.g., Saur et al. 2010). First, the presence of the dense atmosphere prevents any flyby closer than 1,000 km. Second, the almost-perfect alignment of Saturn's magnetic dipole axis with its spin axis prevents large variations of Saturn's magnetic field along Titan's orbit. Third, Titan's ionosphere adds a large external component that must be removed before retrieving the internal component. The Cassini magnetometer team has not reported any evidence of a permanent magnetic field or an inductive one.

During its descent through Titan's atmosphere in January 2005, the Huygens probe measured the horizontal and vertical components of the electric field with the permittivity, wave, and altimetry (PWA) instrument (Béghin et al. 2007). A signal a few hertz wide centered at 36 Hz is present almost continuously throughout the descent. A careful analysis of the data (Simoes et al. 2007) suggested that this signal is of natural origin and would have been the second eigenmode of a Schumann-like resonance in Titan's atmospheric cavity. The Schumann resonance on Earth is the propagation of an electric signal within a cavity limited by two conductive layers that are the ionosphere on the top and the surface (mainly the ocean) at the bottom. The frequency of the resonance is linked to the size of the cavity. On Earth, the Schumann resonance is triggered by powerful atmospheric lightning activity. To date, such a source has not been detected on Titan (Fischer & Gurnett 2011). Another process that could trigger the propagation of the waves is a plasma instability mechanism associated with the corotating Saturnian plasma flow (Béghin et al. 2007, 2012). However, a recent analysis of the signal recorded by the PWA instrument demonstrates a very strong correlation with the history of mechanical vibrations such as parachute release (Lorenz & Le Gall 2020). It seems likely that the PWA signal is due to vibrations of the boom in the electric field present in Titan's atmosphere and cannot be used to infer the depth of an electrically conductive ocean.

During the course of the Cassini-Huygens mission, four independent observations were discussed as evidence for the presence of a deep ocean: obliquity, degree 2 tidal Love number, NSR, and Schumann resonance. Only two of them survived a more thorough analysis: obliquity and degree 2 tidal Love number. The degree 2 gravity coefficients suggest that Titan is differentiated, although not as much as Ganymede, which is consistent with the lack of a permanent magnetic field generated in an iron-rich liquid core. Titan thus consists of a silicate core overlaid by a hydrosphere that includes a deep ocean (**Figure 1**). The next section describes interior structure models that are consistent with EoS for aqueous solutions and silicates.

3. INTERIOR STRUCTURE

3.1. Modeling the Interior Structure

Any model of Titan's interior must satisfy the observational constraints presented in Section 2. Its average density of 1,881 kg/m^3 suggests a large fraction of water ice and other low-density compounds. The interior structure of Titan may consist of up to five main layers (from center to surface): a rocky core, a high-pressure (HP) ice VI–V layer, a liquid water ocean, an ice I shell, and possibly a chemically distinct icy crust enriched in hydrocarbon elements (**Figure 3**). The radius and density of these different layers are determined in order to satisfy the average surface radius, total mass, and MoI factor (**Table 1**). Even if those quantities are well constrained, there are no unique solutions to the problem—different combinations of layer densities and thicknesses can reproduce the observed global values.

In each layer, the mass, gravity, pressure, and MoI are integrated from the material density, which is determined by a given composition/phase using the appropriate EoS (see Section 3.2). The density variations with depth are determined from the pressure and the temperature, which requires the construction of a temperature profile in each layer. The position of the top and bottom ocean interfaces is determined by the intersection of the water ice melting curve and the temperature profile in the ocean (see **Figure 3*a***). Both the melting curve and the ocean adiabat depend on the ocean composition (e.g., Vance et al. 2018).

Due to the physics of the crystallization processes, the outer ice shell and the HP ice layer are believed to be composed of almost pure water ice, for which the density is well known in the pressure range expected in Titan's interior (e.g., Choukroun & Grasset 2010). The main uncertainties are the thickness of the outer ice shell, the density (composition) of the ocean, and the density of the rocky core, which can vary significantly depending on the assumed composition. The ocean composition also affects the melting curves. Owing to its strong depression of the crystallization

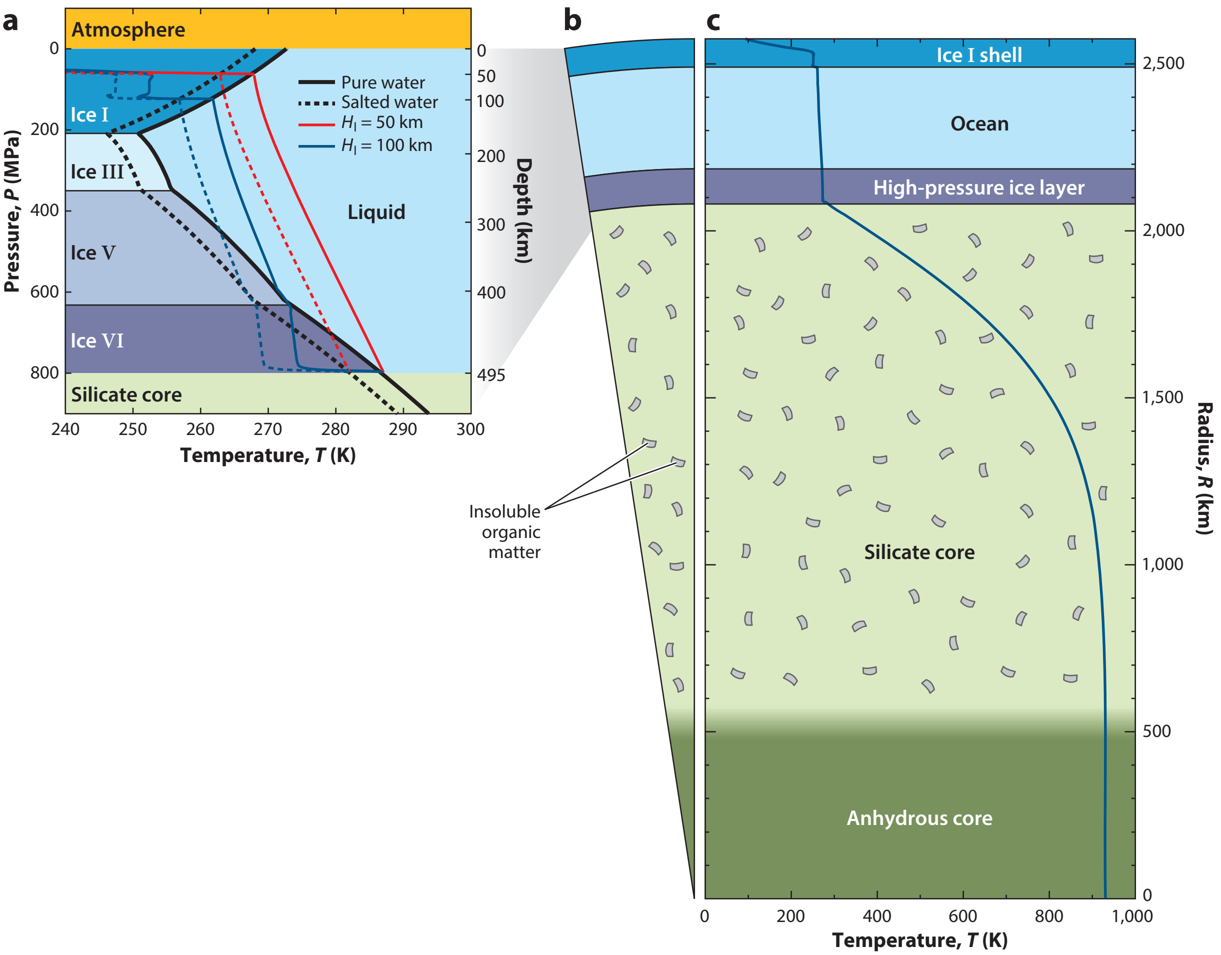

Figure 3

(*a*) Pressure-temperature (*P*-*T*) diagram for conditions in Titan's hydrosphere. Black lines indicate the melting curve for pure H_2O (*solid lines*) (Wagner et al. 1994, 2011) and salty hydrosphere (*dashed lines*) (5 K colder). Red and blue profiles correspond to ice I shell thickness $H_I = 50$ and 100 km, respectively. The depth on the right vertical axis is approximate and corresponds to pure hydrosphere. Panel adapted with permission from Kalousová & Sotin (2020a). (*b*) Interior structure of Titan from Néri et al. (2020). (*c*) A possible temperature profile in Titan (see text for details).

temperature, ammonia has been commonly considered when modeling the evolution of Titan's hydrosphere (Lunine & Stevenson 1987, Grasset & Sotin 1996, Tobie et al. 2005a). These models showed that the presence of a few percent of ammonia would help the preservation of a subsurface ocean inside Titan. A few percent of ammonia, however, reduces the density of the aqueous solution compared to pure water (Croft et al. 1988). This appears incompatible with the estimate of the tidal Love number (Iess et al. 2012, Durante et al. 2019), which points to an ocean denser than pure water. According to the analysis of Mitri et al. (2014) (**Figure 4*b***), the average ocean density should be at least 1,150 kg/m^3 if the ice shell is 50 km thick, and at least 1,190 kg/m^3 for a 100-km-thick convective ice shell. This implies that the ocean should contain a nonwater component that increases the density by about 5% to 10% relative to pure water (**Figure 4*a***). Various compounds have been proposed such as ammonium sulfate (Fortes et al. 2007), sodium chloride,

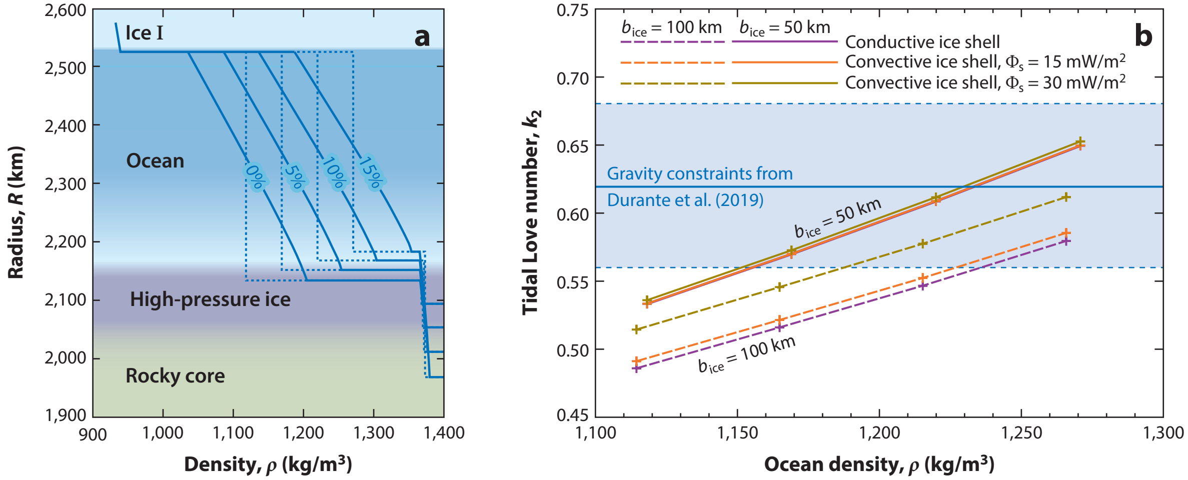

Figure 4

(*a*) Density profiles in the hydrosphere for different oceanic compositions. (*b*) Predicted tidal Love number as a function of average ocean density for two different ice shell thicknesses (50 and 100 km) in a conductive or convective state. Abbreviation: b_{ice}, ice shell thickness. Figure adapted with permission from Mitri et al. (2014).

or magnesium sulfate (Vance et al. 2018). Based on the existing data, it is impossible to determine which one is more likely.

By constraining the hydrosphere structure from the tidal Love number estimate and the phase diagram consideration, it is then possible to determine the size and density of the rocky core from the MoI as explained by Vance et al. (2014) for Ganymede. The MoI factor (C/MR^2) is inferred from the degree 2 gravity coefficients, J_2 and C_{22}, using the Radau-Darwin approximation, which assumes that the gravity field is mostly determined by the dynamical distortion of a radially distributed density structure in response to rotational and tidal forces. The fact that the J_2/C_{22} ratio is not exactly equal to 10/3 (Durante et al. 2019) and the existence of non-negligible higher degree gravity coefficients indicate a departure from the ideal hydrostatic response. As noted in Section 2.2, the topography variations do not correlate with the higher degree gravity coefficients. A global inversion of gravity and topography is required in order to determine the magnitude of the nonhydrostaticity, which would lead to a slightly smaller value of the MoI. The lower the MoI, the larger the differentiation. It seems, however, very unlikely that the MoI would be as low as for Ganymede (0.311), where an iron-rich liquid core is present.

Even small variations in the value of the MoI factor can have major implications for the composition of the rocky core. A value of 0.34 implies a rocky core density of the order of 2,550 to 2,650 kg/m^3 for a core radius ranging between 2,100 and 1,970 km, whereas the density would range between 2,850 and 3,100 kg/m^3 and the radius from 1,950 to 1,770 km for a value of 0.33 (Mitri et al. 2014, Néri et al. 2020). The variability in core density and radius for a given value of the MoI is mostly controlled by the ocean density and the outer ice shell thickness (Mitri et al. 2014). As discussed in Section 3.3, these values of density are smaller than values inferred from the EoS of silicates and iron phases that form carbonaceous chondrites, which are assumed to be one of the building blocks of silicate-rich bodies in the outer Solar System. The low density of the core implies either an incomplete differentiation or a content in iron that would be much less than in carbonaceous chondrites, or the existence of a low-density compound mixed with the rock phase. O'Rourke & Stevenson (2014) performed numerical simulations of double diffusive convection to assess whether Titan could be partially differentiated—i.e., have a mixture of ice and rock in its core. Their study shows that although the differentiation could be delayed, present Titan is not partially differentiated even if ^{40}K, a major component of the radioactive heating, was leached from the core. Similarly, there is no observation or theory that would support an iron content in the building rocks of the Saturnian moons being smaller than in chondrites. The same is true for the Jovian system. If iron concentration is left as a free parameter, it leads to Fe/Si ratios much lower than the chondritic value, but no formation model accounts for large variations of the Fe/Si ratio inferred in Jovian satellites (Sohl et al. 2002). A remaining possibility is a low-density compound of the rocky core for which Néri et al. (2020) proposed that it may be the IOM whose mass fraction could range between 15 and 25 wt% for an MoI factor between 0.33 and 0.34 (**Figure 3*b***). This proposition is consistent with the finding of Miller et al. (2019) that up to 50% of Titan's atmospheric nitrogen comes from the decomposition of IOM. The presence of IOM in Titan's core would have major consequences for the differentiation and evolution of Titan's interior.

3.2. Equations of State of Water and Silicates

Determining the internal structure of Titan compatible with the existing observational constraints requires the use of appropriate EoS for water compounds and silicate minerals. For the pressure and temperature ranges expected in Titan's hydrosphere (1.5 bar to 1 GPa, 100–350 K), several ice polymorphs, aqueous solutions of varying compositions, gas hydrates, and hydrated salts are predicted. Following the pioneering research of Lunine & Stevenson (1987), most of the internal models considered ammonia-water solutions and an NH_3-H_2O phase diagram as representative materials for Titan's hydrosphere. Consequently, the experimental works have been focused on the acquisition of thermodynamic data for the NH_3-H_2O system (Croft et al. 1988, Grasset & Sotin 1996, Hogenboom et al. 1997, Grasset & Pargamin 2005, Choukroun & Grasset 2010). The density constraint provided by Titan's tidal Love number ruled out ammonia as a main constituent of Titan's ocean and suggests rather heavier ionic species such as NaCl, $MgCl_2$, $MgSO_4$, Na_2SO_4, $NH_4(SO_4)_2$, etc.

Quantifying the effect of these ionic species on the thermodynamic properties of aqueous solutions and on the phase diagram of salt-water systems is essential to correctly predict the structure and thermal state of the hydrosphere. The Na-Mg-Cl-SO_4-water systems have been extensively studied below 100 MPa (Journaux et al. 2020b), but, with the exception of the $MgSO_4$-water system (Vance & Brown 2013), they remain poorly known at the higher pressure that is relevant for Titan's hydrosphere. Sound speed measurements at high pressure (Bollengier et al. 2019) are currently under finalization in order to constrain these different salt-water systems. Following the approach developed for pure water systems (Brown 2018, Bollengier et al. 2019), it is possible to derive a Gibbs energy representation of these systems that allows the derivation of the different thermodynamic quantities (density, thermal expansion, heat capacity, chemical potential) relevant for modeling the adiabatic profile through the ocean and the water/ice phase boundaries. The first application using this representation has already been applied to the $MgSO_4$-water system (Vance et al. 2018) and should be generalized in the future to other systems using the SeaFreeze software developed for that purpose (Journaux et al. 2020a).

The density profile in the rocky core can be calculated by using an elementary composition that is consistent with cosmochemical models (Mueller & McKinnon 1988). Alternatively, Néri et al. (2020) took the elementary composition of carbonaceous chondrites from Wasson & Kallemeyn (1988). The density of the silicates is computed using the thermodynamic software Perple_X (Connolly 1990) along a pressure-temperature profile consistent with the conductive heat transfer in a rocky core heated by the decay of the long-lived radioactive elements

Table 2 Characteristics of two possible models of Titan's interior structure

Characteristic	Model 1: convection in the outer ice shell; MoI of 0.341	Model 2: conduction in the outer ice shell; MoI of 0.330
Ocean depth (km)	112	36
Ocean density (kg/m^3)	1,122	1,219
Ocean thickness (km)	250	502
High-pressure ice thickness (km)	130	180
Ocean mass (10^{22} kg)	1.92	4.04
Rocky core radius (km)	2,083	1,856
Rocky core density (kg/m^3)	2,565	2,975
Hydrosphere mass (10^{22} kg)	3.74	5.48
Rocky core mass (10^{22} kg)	9.71	7.97

Model 1 is a nominal pure H_2O model with a thick convective ice shell, whereas Model 2 has a salty ocean (denser) with a thinner conductive crust. Abbreviation: MoI, moment of inertia.

(Castillo-Rogez & Lunine 2010) (**Figure 3*c***). The density of other components (iron sulfide and IOM) is determined from laboratory measurements.

3.3. Comparison Between Different Interior Structure Models

Although the measurements from the Cassini-Huygens mission coupled with the recent laboratory data on the EoS of the different components provide new constraints on Titan's interior structure, there are still a lot of unknowns such as the thickness of the outer ice shell; the presence and distribution of clathrates therein; the thickness, density, and composition of the ocean; the thickness of the HP ice layer; and the composition of the rocky core. **Figure 3*a*** shows a nominal model for a pure H_2O ocean and an ~100-km-thick ice shell (Kalousová & Sotin 2020a). Using the H_2O EoS for the different pressure-controlled phases, one can compute the thickness of the ocean, the thickness of the HP ice layer, and the radius and density of the rocky core. The very low density of the silicate core (2,565 kg/m^3) (**Table 2**) compared to that of carbonaceous chondrites at the relevant (P,T) conditions (**Figure 3*c***) requires the addition of about 25% of IOM. In this model, the temperature profile remains below the dehydration temperature of the silicates (**Figure 3*c***), which suggests that a large fraction of potassium was leached during differentiation. Model 2 has a thinner conductive ice shell, a denser (salty) ocean, and a smaller value of the MoI to account for some potential nonhydrostatic effects (e.g., Durante et al. 2019). This model is also consistent with a value of 0.62 for the tidal Love number (**Figure 4**; **Table 1**). As a result, the radius of the rocky core is smaller, its density is larger but still lower than that of carbonaceous chondrites at these (P,T) conditions, and the thickness of the HP ice layer is larger (**Table 2**). If the salt is sodium chloride that was leached from the rock fraction during differentiation, the amount of chlorine required to get a density of 1,219 kg/m^3 is about 50 times as large as the amount available in the silicates, assuming a carbonaceous chondrite Cl/Si ratio (Wasson & Kallemeyn 1988). However, the space of possible models is quite large. Further studies are required to investigate the most likely interior model that can satisfy all the information available for Titan.

4. INTERNAL DIFFERENTIATION AND EVOLUTION

4.1. Accretion and Formation of a Primitive Ocean and Atmosphere

During the very early stage of Titan's evolution, the accretional (impact) heating is the predominant heat source and determines the initial structure and postaccretional thermal state of Titan's

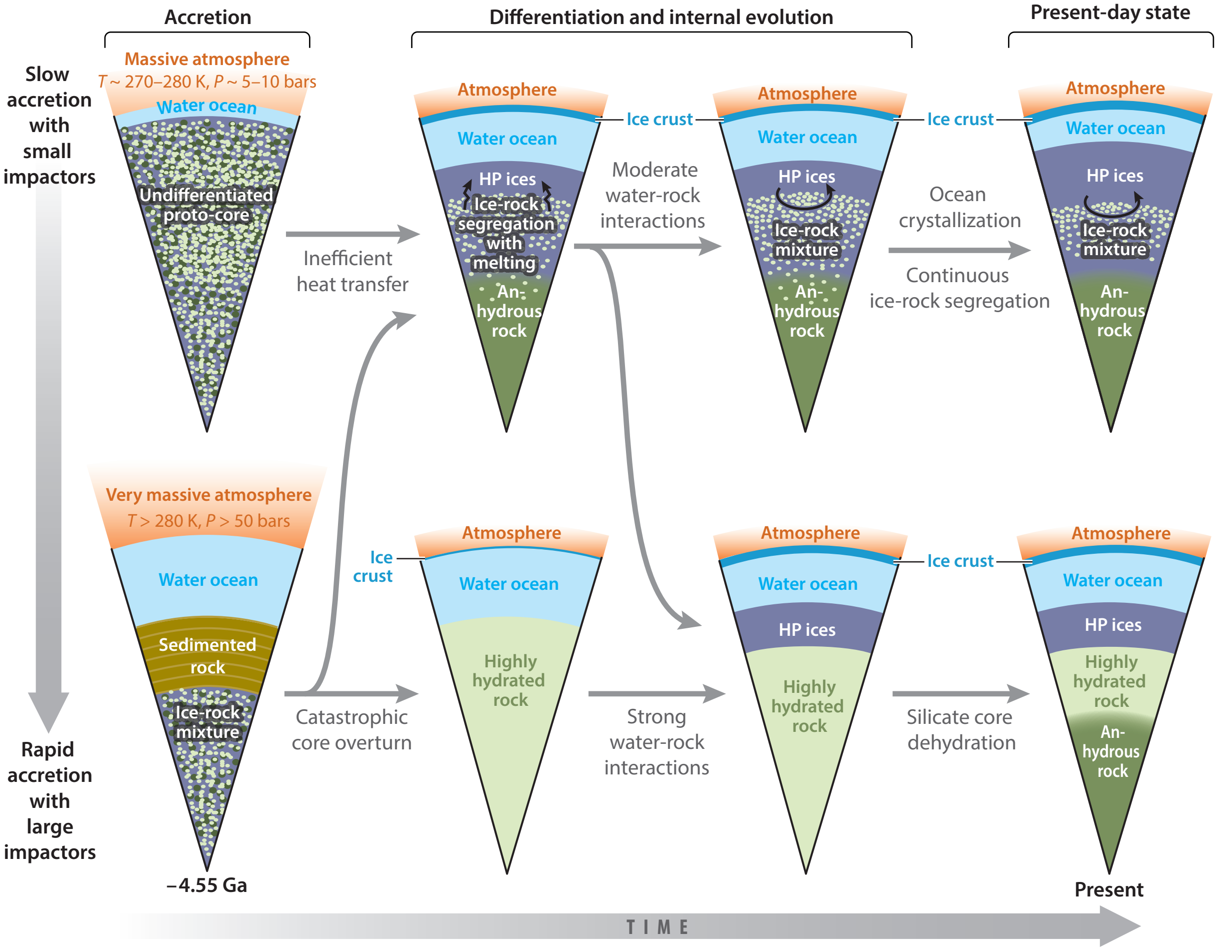

Figure 5

Possible evolution scenarios for the interior of Titan for different initial states. Depending mostly on the efficiency of heat transfer in the interior, different bifurcations in the evolutionary path may have occurred. Abbreviation: HP, high pressure. Figure adapted with permission from Tobie et al. (2014).

interior (**Figure 5**). The impact heating results from the deposition of impactor kinetic energy during the satellite accretion, and it thus depends on the impactor velocity as well as on the fraction of kinetic energy that is converted into heat. The impact creates a shock wave that compresses the satellite—below the impact site, the peak pressure is almost uniform in a quasi-spherical region called the isobaric core (e.g., Croft 1982, Senshu et al. 2002). Energy balance between the impactor kinetic energy and the impact heating leads to a local temperature increase proportional to the square of the growing icy moon radius (e.g., Monteux et al. 2007). As long as the growing moon radius is below 1,000 km, the local temperature increase is less than 10–15 K after each impact. Above 2,000 km, the increase of temperature is larger than 50 K. During accretion, the global increase of surface temperature depends on how deep the energy is buried, which is controlled by the impactor size, and how frequently the successive impacts occurred.

By modeling the satellite accretion in three dimensions from a swarm of impactors of various sizes, Monteux et al. (2014) tested the influence of impactor size distribution on the thermal evolution of a growing satellite. They showed that for satellites exceeding 1,500–2,000 km, surface melting can be avoided only if the satellite accreted relatively slowly (>1 Myr) from small impactors (<1 km) and if the conversion of impact energy into heat is unrealistically inefficient (<10–15%), confirming the earlier estimations of Barr et al. (2010). However, as soon as a small fraction (>10%) of the impactors exceeds 1 km, global melting of the outer layer of the growing satellite cannot be avoided. As a result, a surface ocean forms that is in equilibrium with a massive primitive atmosphere generated by the release of volatiles brought by the icy impactors (Kuramoto & Matsui 1994, Marounina et al. 2018).

The volume of the surface ocean depends on the efficiency of accretion processes. For a slow accretion with small impactors, melting occurs at the end of accretion, resulting in the formation of a few tens of kilometers thick ocean and an atmosphere of less than 10 bars. However, for rapid accretion with large impactors, melting could occur when the satellite radius reached 1,000 km (about 40% of its final radius and less than 10% of its final mass), leading to the formation of a very thick water layer in equilibrium with an atmosphere with the surface pressure exceeding 50 bar (Tobie et al. 2012, 2014). Marounina et al. (2018) showed that the atmosphere originating from the devolatilization of icy impactors was mostly composed of CO_2 and CH_4, which contrasts with the present N_2-dominated atmosphere. Melting of infalling icy impactors also released rock particles that sedimented at the base of the ocean. During this postaccretional period, the pressure at the base of the ocean was not large enough to lead to the formation of an HP layer and the water ocean directly interacted with the sedimented rock layer, potentially promoting large-scale water-rock interactions and production of CH_4 and other gas compounds (Glein 2015).

4.2. Heat Budget and Water-Ice-Rock Segregation

Saturn likely formed after Jupiter (e.g., Sasaki et al. 2010), so when Titan formed, most of the short-lived radioactive isotopes (mainly ^{26}Al) were already decayed and did not contribute significantly to the early internal heat budget. The main heat source was provided by the decay of long-lived radiogenic elements, mostly ^{40}K and ^{235}U, during the first billion years. To estimate the heat power generated by the radiogenic decay of the rock phase in the moons, chondrites can be used. For Titan, carbonaceous chondrites, which are believed to be the dominant type of chondrites beyond Jupiter (Kruijer et al. 2017), are commonly assumed to be a good proxy of the rock phase (Fortes 2012, Tobie et al. 2012, Glein 2015, Néri et al. 2020). Assuming a composition dominated by CI chondrites, the total radiogenic power just after accretion is estimated to be about 2.5 TW and progressively decays with time to ∼300 GW at present (Hussmann et al. 2010).

Heat generated by tidal friction inside Titan due to the gravitational interaction with Saturn may have also significantly varied during Titan's history. Contrary to the Jupiter system where the Laplace resonance forces the moons' eccentricity, the absence of strong orbital resonance forcing Titan's eccentricity suggests that the eccentricity of Titan, which is already large (∼3%), was even larger in the past, potentially resulting in tidal heating comparable to Europa's (Tobie et al. 2005b). The recent analysis of Lainey et al. (2020) further indicates that Titan may have formed much closer to Saturn and migrated outward due to resonance locking with Saturn. At present, the global dissipation in Titan is estimated to be less than 200 GW (Tobie et al. 2005b, Kalousová & Sotin 2020b), but it may have been much larger in the past, potentially exceeding several terawatts. During the very early stage, Titan also experienced strong tidal despinning before reaching the tidally locked spin-orbit resonance. Although the associated dissipation rate is very large, it lasted for short periods of time, on the order of 100,000 years (Hussmann et al. 2010), resulting in a moderate increase of internal temperature of 25 to 50 K (Tobie et al. 2014).

A third source of energy resulted from the release of gravitational energy associated with the internal differentiation (Friedson & Stevenson 1983, Hussmann et al. 2010). An approximate estimate of the temperature increase due to viscous heating associated with the ice-rock separation can be obtained by considering the difference of gravitational energy between an initially homogeneous interior and a differentiated interior with a full separation of rock and ice phases. This corresponds to a maximum potential temperature increase on the order of 100 to 150 K (Tobie et al. 2014) assuming no heat loss. The total heat budget, including radiogenic heating, tidal viscoelastic heating, and viscous heating, determines the timing of the differentiation process. Enhanced tidal dissipation may, for instance, trigger an earlier differentiation process and was suggested to explain the difference in differentiation state between Callisto and Ganymede (Showman & Malhotra 1999).

If the ice-rock separation is fast enough (<0.5 Gyr), the dissipation of potential energy may induce runaway melting and thus lead to a catastrophic differentiation, as proposed for Ganymede (Friedson & Stevenson 1983, Kirk & Stevenson 1987). This corresponds to the scenario shown in **Figure 5** (second row). If the differentiation process is slower and more gradual (>1 Gyr), the convective heat transfer should be able to transport the additional energy and prevent internal melting, as proposed for Callisto (Nagel et al. 2004). More recently, O'Rourke & Stevenson (2014) showed that double-diffusive convection in a mixed ice-rock interior can delay internal melting and ice-rock separation but cannot prevent it, even if reduced radiogenic power is assumed (see **Figure 5**, first row). This indicates that it is difficult to prevent full separation between the rock and the hydrosphere. We should keep in mind, however, that the duration of the differentiation process depends on the rheology of ice-rock mixtures, which is poorly constrained at high pressures. Further experimental and modeling efforts are required to better understand the differentiation processes of large icy moons.

4.3. Water-Rock Interactions and Conditions for the (Non)formation of an Iron Core

After the separation of rock and ice, water-rock interactions are limited to the ice-rock interface at the base of the HP layer. Even though water at this interface is mostly in the form of an HP ice phase owing to the elevated pressure (>0.8–1 GPa), liquid water may locally exist and potentially circulate through the upper part of the rocky core. Depending on the efficiency of heat transfer through the HP ice layer, which is mostly controlled by the poorly known viscosity of HP ice (Kalousová et al. 2018; see also Section 5), the formation of transiently present liquids at the rock-ice interface may be possible (Kalousová & Sotin 2020a). These liquids could interact with the underlying rocks before percolating upward to the ocean. Warm liquid water may also be released from the core when the dehydration temperature is reached (Castillo-Rogez & Lunine 2010). This dehydration event may have occurred relatively late during Titan's evolution (>3–3.5 Gyr after formation), provided that sufficient amounts of radiogenic potassium were leached from the core and that thermal diffusivity in the core is not too low (Castillo-Rogez & Lunine 2010). In the warm evolution scenarios, intensive water-rock interactions were likely during two main sequences of Titan's evolution—before 1 Gyr during the differentiation and after 3–3.5 Gyr during the core dehydration.

Dehydration processes may not occur if the hydrated silicate core can convect, thus removing the radioactive heat efficiently. Hydrated silicates have a deformation rate that strongly depends on stress and only weakly on temperature (Hilairet et al. 2007). To date, no study has investigated the possibility of convection in the hydrated silicates. If convection does not start in the hydrated silicates, then dehydration may start in the center of the moon (Castillo-Rogez & Lunine 2010). The dehydration temperature is 350 K lower than the eutectic temperature of the Fe-FeS system [1,200 K at Titan's interior pressure (Buono & Walker 2011)]. If the amount of internal heating is large enough, then the temperature may exceed the Fe-FeS system eutectic temperature and an iron core may form, a process that may have happened on Ganymede (Bonnet-Gibet et al. 2020). The lack of an intrinsic magnetic field at Titan indicates that such high temperatures may not have been reached inside Titan.

5. DYNAMICS AND EVOLUTION OF THE HYDROSPHERE

Based on the interior structure models, Titan's hydrosphere is about 500 km thick (see Section 3). It harbors a subsurface water ocean that is sandwiched between the outer ice shell and a deep ice layer possibly composed of several HP ice phases (ices VI, V, and III) (see **Figure 3**). We first review recent models describing the dynamics and heat transfer in the particular hydrosphere layers before addressing the coupled evolution of the hydrosphere as a whole.

5.1. Dynamics of the High-Pressure Ice Layer

Titan's HP ice layer is supplied with radiogenic heat flow from the underlying silicate core (Section 4), and its top boundary is determined by the intersection of the ocean adiabat and the melting curve (Section 3). Its dynamics is mainly controlled by the HP ice viscosity, which has been measured by several groups (Sotin et al. 1985; Sotin & Poirier 1987; Durham et al. 1996, 1997; for a compilation, see also Journaux et al. 2020b). The temperature difference between the bottom and top boundaries is less than ~30 K (**Figure 3**), and thus the ice temperature is always close to the melting curve. This has two implications. First, the viscosity is low enough for thermal convection to occur (Choblet et al. 2017b, Kalousová & Sotin 2020a). Second, the melting temperature is reached for a broad range of models (Choblet et al. 2017b), and thus a two-phase mixture model is necessary to self-consistently treat the melting process and the subsequent melt evolution. **Figure 6** shows a snapshot from a two-phase convection simulation tailored to Titan's HP ice layer by Kalousová & Sotin (2020a). **Figure 6*a*** depicts the temperature difference from the melting temperature (note that $\Delta T \leq 20$ K), with the dark red denoting the partially molten (temperate) ice where temperature equals the melting temperature ($T = T_{\mathrm{m}}$) and where some water may be present. **Figure 6*b*** shows the corresponding water content (porosity Φ)—note

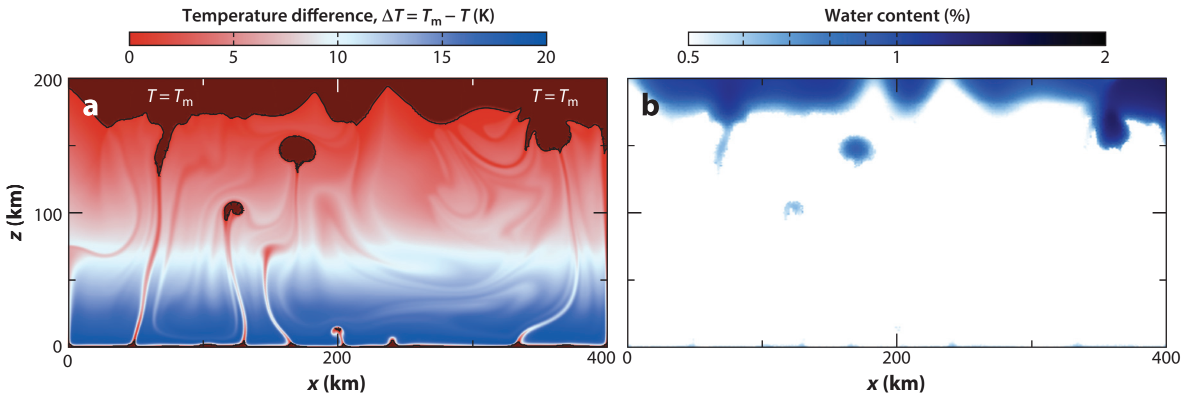

Figure 6

Heat and water transport through Titan's high-pressure ice layer. (*a*) Temperature difference from the melting temperature ($\Delta T = T_{\mathrm{m}} - T$). Dark red marks the temperate ice ($T = T_{\mathrm{m}}$). (*b*) Water content (porosity). Figure adapted with permission from Kalousová & Sotin (2020a).

that only a few percent are present, and no melt accumulation is observed. Due to the decrease of the melting temperature with the decreasing pressure [i.e., increasing vertical coordinate (see **Figure 3**)], most of the water is produced in the top layer of temperate ice at the ocean interface from where it is extracted into the ocean. Due to this temperate layer, no cold thermal boundary layer (TBL) is present and the convection is thus characterized by the hot upwelling plumes generated in the hot TBL and a passive downwelling. Some water may also be present in the upwelling plumes and at the silicates' interface. Scaling performed by Kalousová & Sotin (2020a) showed that the occurrence or not of bottom melting mainly depends on the incoming heat flux, the ice viscosity, and the HP ice layer thickness. For the currently expected interior structure (Section 3), the amount of heat produced in the core (Section 4), and reasonable viscosity values, Kalousová & Sotin (2020a) predict that melt may be present at the interface of Titan's core and HP ice layer. This has profound astrobiology implications because volatiles and organics present in Titan's core may be leached and transported by the liquids into the ocean (Section 4). This makes Titan quite different from Ganymede, whose HP ice layer is probably much thicker and melt is not currently predicted at its bottom (Kalousová & Sotin 2018, Kalousová et al. 2018). Let us note that all the described models were performed assuming a pure H_2O setting. If other compounds such as ammonium sulfate, magnesium sulfate, or sodium chloride are present in the ocean (Section 3), the processes described above may be altered because the melting temperatures as well as the liquid densities would be changed substantially.

5.2. Dynamics of the Ocean

Flows in Titan's subsurface ocean can be driven by thermo-compositional convection as well as mechanically by tides (for a review, see Soderlund et al. 2020). For the rotating subsurface oceans, the convective heat transfer efficiency and the outgoing heat flux pattern depend strongly on the particular importance of driving buoyancy, Coriolis, and inertia forces when compared to retarding viscous forces (e.g., Gastine et al. 2016, Soderlund 2019, Amit et al. 2020) (**Figure 7**). Amit et al. (2020) described two distinct regimes: (*a*) equatorial cooling characterized by a dominant top boundary heat flux in the equatorial region, which was found for cases when rotation was important, and (*b*) polar cooling characterized by dominant top boundary heat flux at polar regions found for cases when rotation was less important (see **Figure 7**). The expected range of Ekman and Rayleigh numbers relevant to Titan's ocean (**Figure 7**) suggests a rather limited effect of rotation on its dynamics, consistent with the polar cooling pattern. These results are in agreement with the findings of Kvorka et al. (2018), who predicted dominant heat fluxes at the poles to explain Titan's long-wavelength topography (see also the next section for more details). Using the same spectral code as Amit et al. (2020), Soderlund (2019) found rather different results with the largest polar heat flux (i.e., polar cooling) for cases with a strong influence of rotation and equatorial heat flux peaks (i.e., equatorial cooling) for a more moderate rotational influence. This obvious contradiction between their findings may be the result of a different choice of mechanical boundary conditions—while Soderlund (2019) prescribed impenetrable, stress-free boundaries, Amit et al. (2020) used rigid boundaries. Similarly, the effect of thermal boundary conditions should be carefully investigated because in both studies, isothermal boundaries were prescribed. However, given that the ocean is sandwiched between two ice layers (HP ice layer below and ice I shell above) with much slower dynamics, the incoming and outgoing heat fluxes are likely to be governed by the dynamics of these two solid layers—i.e., prescribed incoming and outgoing heat fluxes would be more appropriate boundary conditions than prescribed temperature. A dedicated numerical study investigating these different settings would certainly bring more insight into the ocean dynamics of Titan as well as other ocean worlds.

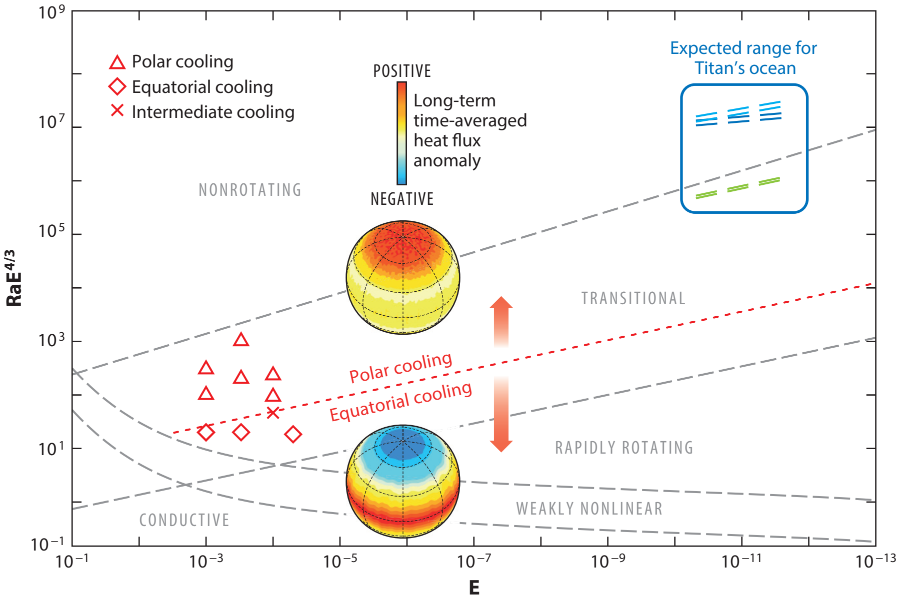

Figure 7

Regime diagram proposed by Gastine et al. (2016) showing the different regimes for convecting rotating flows in a spherical shell depending on Ekman number (E; ratio of viscous and Coriolis forces) and product of Rayleigh number and Ekman number to the 4/3 (Ra; ratio of thermal buoyancy to momentum and heat diffusion). The blue box highlights the expected values for Titan's ocean (*dashed colored lines*) (for more details, see Amit et al. 2020). Results by Amit et al. (2020) are denoted by red diamonds (equatorial cooling), red triangles (polar cooling), and a red cross (intermediate cooling). The inserted spheres depict the long-term time-averaged heat flux anomaly (i.e., heat flux with respect to the mean value) across the ocean top boundary. Figure adapted with permission from Amit et al. (2020).

Titan's eccentric orbit and nonzero obliquity result in time-variable tidal forcing that drives ocean flow. For Europa, the associated tidal dissipation was suggested as an important source of energy by Tyler (2008), although the assumed value of tidal quality factor remained debatable. To provide an independent constraint on the possible amount of ocean tidal dissipation, Chen et al. (2014) used the shallow-water equations that neglect the radial ocean currents with respect to horizontal currents (making the problem a 2D one) with an Earth-like value of bottom drag coefficient. They also neglected the effect of the overlying ice shell. Their results show that the dissipated power in Titan's ocean due to obliquity tides is on the order of 10 GW, which was later confirmed by Hay & Matsuyama (2017). The corresponding surface heat flux of about 0.1 mW/m^2 is, however, negligible compared to the tidal heating in solid layers as well as to the radiogenic heating in the core (Chen et al. 2014) (see also Section 4). The inclusion of the outer ice shell covering the ocean has a minor effect on both the eccentricity and the obliquity tidal heating in Titan's ocean. Recently, Rovira-Navarro et al. (2019) and Rekier et al. (2019) performed simulations tailored to Europa and Enceladus that took into account the three-dimensional (3D) nature of ocean flows. Although the observed pattern of periodic inertial waves differed from the shallow-water results, the tidal dissipation due to these inertial waves was found to be negligible when compared to the traditional heat sources. Finally, let us note that future studies should also investigate the interaction between convection and the tidally driven flows (Soderlund et al. 2020).

5.3. Dynamics of the Outer Ice Shell

The thermal state of Titan's outer ice shell is not well constrained. Depending on its thickness and the ice viscosity, heat can be transferred by either conduction (thin shells, large viscosity) or convection (thick shells, small viscosity). The viscosity is mainly determined by the ice grain size (Durham & Stern 2001, Durham et al. 2001, Goldsby & Kohlstedt 2001), which may vary from less than 1 mm to more than a few millimeters and would evolve dynamically (Barr & McKinnon 2007). Therefore, the critical thickness for the convection to occur depends mainly on the ice grain size, often represented by the viscosity value at the melting temperature, η_0. Lefevre et al. (2014) found that Titan's 100-km-thick ice shell is likely to convect unless $\eta_0 \gtrsim 3 \times 10^{16}$ Pa·s, roughly corresponding to a 7-mm grain size. If the shell is 50 km thick, the threshold viscosity would be about one order of magnitude smaller, corresponding to a 3-mm grain size. The heat transfer by convection is far more efficient than the conductive cooling and leads to an efficient crystallization of the deep ocean unless another mechanism is acting to delay the freezing.

The presence of ammonia has been suggested (e.g., Grasset & Sotin 1996), which would decrease the ocean temperature, thus increasing viscosity and making convection less efficient or not occur at all. However, a significant ammonia concentration would be necessary to substantially decrease the ocean temperature, which is not compatible with the densities inferred by Mitri et al. (2014) as well as with the recent research by Leitner & Lunine (2019), who suggest that only up to about 5% of ammonia could be present in Titan's ocean. Another possibility is tidal heating in the ice shell or the core that keeps oceans liquid in bodies such as Europa or Enceladus (Tobie et al. 2005b, Choblet et al. 2017a). However, given the high value of Titan's eccentricity and no resonance to maintain it on geological timescales, it is not likely that significant dissipation is currently occurring in Titan's interior (Tobie et al. 2005a,b), although more energy could have been dissipated earlier in the evolution (Section 4). Alternatively, a crust made of methane clathrates—that have about ten times smaller thermal conductivity than ice under Titan's surface conditions (Sloan & Koh 2007)—has been proposed to insulate Titan's interior and delay the ocean crystallization (e.g., Loveday et al. 2001, Tobie et al. 2006). Recently, Kalousová & Sotin (2020b) revisited this concept and performed simulations of thermal convection in Titan's clathrate capped ice shell. **Figure 8** shows the comparison of temperature for simulations without clathrates (panel *a*) and with a 10-km-thick clathrate crust (panel *c*). Panel *b* shows the average temperature profiles for

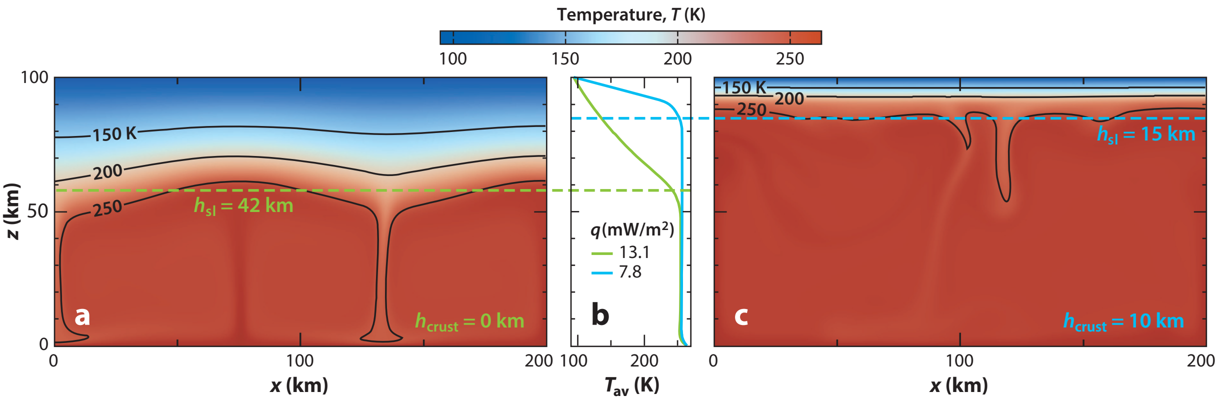

Figure 8

Comparison of temperature fields assuming a clathrate crust (*a*) 0 km and (*c*) 10 km thick. Panel *b* shows the average temperature profiles (*full lines*). The dashed lines indicate the stagnant lid (h_{sl}). Figure adapted from Kalousová & Sotin (2020b).

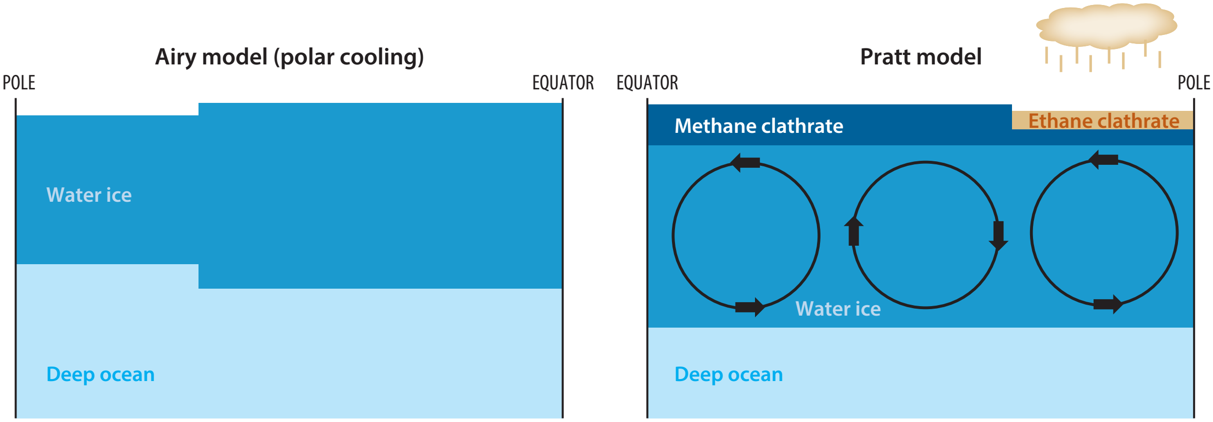

Figure 9

Models of ice I shell that can explain the observed gravity and topography data: (*a*) Airy model (Nimmo & Bills 2010). (*b*) Pratt model (Choukroun & Sotin 2012).

these two cases. The inclusion of the clathrate crust results in (*a*) a significant reduction of the stagnant lid thickness (h_{sl})—in this particular setting from 42 km ($h_c = 0$ km) to 15 km ($h_c = 10$ km)—and (*b*) a substantial decrease in the amount of heat extracted from Titan's ocean (q)—for the depicted case by about 40%. As a consequence of the thinner stagnant lid, a warm material is brought closer to Titan's surface, which may facilitate material exchange with the surface, e.g., due to cryovolcanism (Mitri et al. 2008, Lopes et al. 2013).

As discussed in Section 2, Titan's long-wavelength topography is characterized by polar depressions of about 300 m, and the negligible correlation of topography with the gravity field anomalies points to a high degree of compensation (Durante et al. 2019). A concept of isostasy has been considered to explain the observed topography. Nimmo & Bills (2010) assumed that Titan's shell is rigid and conductive and proposed that lateral ice shell thickness variations (corresponding to Airy isostasy) can lead to topographies that fit well in the observations (**Figure 9*a***). The topic was further investigated by Lefevre et al. (2014) and Kvorka et al. (2018) who found that lateral flows driven by the shell thickness variations would tend to remove any ice shell/ocean interface topography unless the ice viscosity at the base of the shell exceeds 10^{16} Pa·s, corresponding to either a coarse grain size (greater than or equivalent to several millimeters) or a very cold ocean ($\lesssim$240 K). As discussed above, a cold ammonia-rich ocean is not compatible with the high value of k_2 (Section 3). Kvorka et al. (2018) further showed that Titan's topography cannot be reproduced by the pattern of tidal heating in the ice shell as initially proposed by Nimmo & Bills (2010). Their results, however, indicated that Titan's polar flattening could be explained by lateral variations of ocean heat flux with amplitudes between 0.1 and 1 mW/m^2, warm water upwellings at the poles, and cold downwellings close to the equator. Such a pattern would agree with the polar cooling of Amit et al. (2020) (see previous section). Alternatively, Choukroun & Sotin (2012) proposed that the polar depressions could be explained by subsidence due to the presence of ethane clathrate that is about 8% denser than water ice [corresponding to Pratt isostasy (**Figure 9*b***)]. This model is supported by the observation of ethane rains at the poles (Griffith et al. 2006). The ethane polar caps would be the ethane reservoir that could explain the absence of atmospheric ethane, although it is the main product of methane photolysis in the upper atmosphere (e.g., Lavvas et al. 2008). The ethane clathrate would form by substitution of methane by ethane in the methane clathrate crust, a process observed in laboratory experiments (Murshed et al. 2010), or by the reaction of liquid ethane with water ice as observed experimentally by Vu et al. (2020).

5.4. Coupled Evolution of the Hydrosphere and Implications for the Atmosphere

As stated by Mitchell & Lora (2016), models need to consider the interactions between Titan's atmosphere, surface, and subsurface in order to make further progress in understanding Titan's complex climate system. The greatest mystery is how Titan can retain an abundance of atmospheric methane with only limited surface liquids, while methane is being irreversibly destroyed by photochemistry. A related mystery is how Titan can hide all of the ethane that is produced in this process (Lavvas et al. 2008). All along Titan's history, the evolution of the hydrosphere has likely influenced the composition of the atmosphere, by controlling the outgassing rate (e.g., Tobie et al. 2006) and possible internal recycling of hydrocarbon compounds (e.g., Choukroun & Sotin 2012). The hydrosphere may contain large quantities of volatiles, either dissolved in the ocean or stored in the form of gas clathrate hydrates in the icy shell (Choukroun et al. 2010, 2013; Tobie et al. 2012).

The release of these volatile compounds is, however, limited due to their solubility in the internal ocean and the clathration processes within the H_2O layers. Outgassing from the interior may occur through two different mechanisms: (*a*) destabilization of clathrates stored in the outer ice shell by thermal convective plumes or by impacts and (*b*) mobilization of dissolved gas molecules contained in the water ocean and subsequent bubble formation if the ocean gets saturated (Tobie et al. 2006, 2009). Both processes are controlled by methane because it is expected to be the dominant gas in the form of clathrate hydrate in the crust and because it is the only gas compound that may reach the saturation point in the ocean during periods of reduced ice shell thicknesses. The amount of ^{40}Ar detected in the atmosphere provides constraints on the level of methane outgassing through time. Owing to its low solubility in water, argon should be preferentially incorporated in CH_4-rich bubbles when they form at the ocean-ice interface and should then be transported upward by the percolating CH_4-rich fluids. Following this extraction mechanism, Tobie et al. (2012) estimated that the atmospheric mass of methane has been renewed at least 20–30 times during Titan's evolution in order to explain the atmospheric abundance of ^{40}Ar as detected by Huygens (Niemann et al. 2010).

Following the evolution scenario proposed by Tobie et al. (2006), the outgassing of methane may result in episodic destabilization of the methane clathrate reservoir, accumulated in the crust during the differentiation process. This crust would then thin in response to the release of heat associated with the core evolution (Tobie et al. 2006), resulting in the dissolution of methane in the ocean and the outgassing of the gas in excess (Tobie et al. 2009). According to this scenario, several kilometers of methane clathrates may still be present in the outer icy shell, limiting the cooling rate of the ocean (Kalousová & Sotin 2020b). Recent thermal destabilizations of this reservoir may explain the present-day atmospheric methane (Tobie et al. 2006). This evolution model was based on a simplified 1D approach, assuming an ammonia-water ocean and ignoring the coupling between the ocean and the HP ice layer. More sophisticated evolution models considering the latest advances in physical and thermodynamic description of the hydrosphere should be developed to better understand the impact of the hydrosphere evolution on the atmosphere. The recent advances made in the description of the large-scale dynamics of the HP ice layer (Section 5.1) and of the ocean (Section 5.2) motivate the need for developing a new generation of models describing the exchange processes between the different layers in a 3D framework and using a consistent thermodynamic approach for phase changes and chemical exchanges between each layer of the hydrosphere.

6. DISCUSSION AND CONCLUSIONS

The Cassini-Huygens mission has provided key information on Titan's interior structure such as the presence of a deep ocean, the near-hydrostatic equilibrium of its long-wavelength topography, and the low density of its rocky core. Titan is almost the same size and mass as Ganymede, Jupiter's largest moon, but the apparent absence of an inner iron-rich core seems to indicate that Titan's rocky core did not experience temperatures as high as in Ganymede. The upcoming JUpiter ICy moons Explorer (JUICE) mission managed by the ESA (launch expected in 2022) will orbit Ganymede and provide a unique set of gravity, topography, rotation, electromagnetic field, and radar sounder measurements. These data will provide a very good picture of Ganymede's interior structure. The comparison between the two moons may help us understand the interior structure and thermal evolution of each of them.

The habitability requirements for a planet or a moon include water, essential elements (carbon, hydrogen, nitrogen, oxygen, phosphorus, sulfur), chemical energy, and time (Cockell et al. 2016). The Cassini-Huygens mission demonstrated that Titan has a deep ocean. The thermal evolution included several episodes when water and rocks interacted and most likely left elements in the ocean. Organic material forms in the atmosphere, and after falling on the surface, it may be transferred to the deep ocean. As discussed in Section 2.4 (atmospheric constraints) and in Section 5.1 (HP ice layer dynamics), exchanges have occurred between the rocky core and the atmosphere, implying that transfers of volatiles and other elements coming from the decomposition of IOM in the core have existed between the rocky core and the ocean. Whether the transfer from the surface to the ocean and the transfer from the rocky core to the ocean can provide the chemical disequilibrium and chemical energy that could lead to life is an open issue.

Models describing the geological evolution of Titan must consider all the information that has been acquired with the Cassini-Huygens data as well as the results of laboratory experiments. Tobie et al. (2006) proposed a model that was consistent with the amount of methane in the atmosphere, the presence of a deep ocean, the large eccentricity, and the mass. New information from Cassini, the recent progress on EoS, and other key parameters of the compounds that built Titan, as well as recent advances in the modeling of multiphase layers, point to the development of a new thermal evolution model. Such a model would be useful to define questions that could be answered by the upcoming Dragonfly mission (Turtle et al. 2017) that will explore Selk crater (**Figure 2**). Questions such as the presence or not of a clathrate crust, the thickness of the ice shell, and the tectonic activity of Titan may be answered thanks to the geophysical package onboard that mission (Lorenz et al. 2019). It will shed more light on Titan, the satellite that resembles Earth more than any other.

DISCLOSURE STATEMENT

The authors are not aware of any affiliations, memberships, funding, or financial holdings that might be perceived as affecting the objectivity of this review.

ACKNOWLEDGMENTS

The authors thank Dr. Benoit Seignovert for processing the Titan's color image (**Figure 2*b***), Prof. Ondřej Čadek for providing the topography map (**Figure 2*a***), and the reviewer for a careful reading. Part of this work was carried out at the Jet Propulsion Laboratory (JPL), California Institute of Technology, under a contract with NASA. This work was partially supported by the NASA Astrobiology Institute through its JPL-led team named Habitability of Hydrocarbon Worlds: Titan and Beyond (17-NAI8_2-0017). K.K. was supported by the Czech Science Foundation through project No. 19-10809S and by Charles University Research Program No. UNCE/SCI/023. G.T. acknowledges support from the French Agence Nationale de la Recherche ANR (OASIS project, ANR-16-CE31-0023-01). CNES support for the processing of the Cassini/VIMS data is acknowledged.

LITERATURE CITED

Amit H, Choblet G, Tobie G, Terra-Nova F, Čadek O, Bouffard M. 2020. Cooling patterns in rotating thin spherical shells—application to Titan's subsurface ocean. *Icarus* 338:113509

Baland R-M, Tobie G, Lefevre A, Van Hoolst T. 2014. Titan's internal structure inferred from its gravity field, shape, and rotation state. *Icarus* 237:29–41

Baland R-M, Van Hoolst T, Yseboodt M, Karatekin Ö. 2011. Titan's obliquity as evidence of a subsurface ocean? *Astron. Astrophys.* 530:A141

Barnes JW, Brown RH, Radebaugh J, Buratti BJ, Sotin C, et al. 2006. Cassini observations of flow-like features in western Tui Regio, Titan. *Geophys. Res. Lett.* 33(16):L16204

Barr AC, Citron RI, Canup RM. 2010. Origin of a partially differentiated Titan. *Icarus* 209(2):858–62

Barr AC, McKinnon WB. 2007. Convection in ice I shells and mantles with self-consistent grain size. *J. Geophys. Res.* 112(E2):E02012

Béghin C, Randriamboarison O, Hamelin M, Karkoschka E, Sotin C, et al. 2012. Analytic theory of Titan's Schumann resonance: constraints on ionospheric conductivity and buried water ocean. *Icarus* 218(2):1028–42

Béghin C, Simoes F, Krasnoselskikh V, Schwingenschuh K, Berthelier JJ, et al. 2007. A Schumann-like resonance on Titan driven by Saturn's magnetosphere possibly revealed by the Huygens Probe. *Icarus* 191(1):251–66

Bézard B. 2014. The methane mole fraction in Titan's stratosphere from DISR measurements during the Huygens probe's descent. *Icarus* 242:64–73

Bills BG, Nimmo F. 2008. Forced obliquity and moments of inertia of Titan. *Icarus* 196(1):293–97

Bills BG, Nimmo F. 2011. Rotational dynamics and internal structure of Titan. *Icarus* 214(1):351–55

Bollengier O, Brown JM, Shaw GH. 2019. Thermodynamics of pure liquid water: sound speed measurements to 700 MPa down to the freezing point, and an equation of state to 2300 MPa from 240 to 500 K. *J. Chem. Phys.* 151(5):054501

Bonnet-Gibet V, Choblet G, Sotin C, Vance SD, Guignard J, Tobie G. 2020. *Thermal and chemical evolution of Ganymede's primitive core*. Paper presented at the European Planetary Science Congress 2020, online, Sept. 21–Oct. 9

Brown JM. 2018. Local basis function representations of thermodynamic surfaces: water at high pressure and temperature as an example. *Fluid Phase Equilib.* 463:18–31

Buono AS, Walker D. 2011. The Fe-rich liquidus in the Fe-FeS system from 1 bar to 10 GPa. *Geochim. Cosmochim. Acta* 75(8):2072–87

Castillo-Rogez JC, Lunine JI. 2010. Evolution of Titan's rocky core constrained by Cassini observations. *Geophys. Res. Lett.* 37:L20205

Chen E, Nimmo F, Glatzmaier G. 2014. Tidal heating in icy satellite oceans. *Icarus* 229:11–30

Choblet G, Tobie G, Sotin C, Běhounková M, Čadek O, et al. 2017a. Powering prolonged hydrothermal activity inside Enceladus. *Nat. Astron.* 12:841–47

Choblet G, Tobie G, Sotin C, Kalousová K, Grasset O. 2017b. Heat transport in the high-pressure ice mantle of large icy moons. *Icarus* 285:252–62

Choukroun M, Grasset O. 2010. Thermodynamic data and modeling of the water and ammonia-water phase diagrams up to 2.2 GPa for planetary geophysics. *J. Chem. Phys.* 133(14):133402

Choukroun M, Grasset O, Tobie G, Sotin C. 2010. Stability of methane clathrate hydrates under pressure: influence on outgassing processes of methane on Titan. *Icarus* 205(2):581–93

Choukroun M, Kieffer SW, Lu X, Tobie G. 2013. Clathrate hydrates: implications for exchange processes in the outer Solar System. In *The Science of Solar System Ices. Astrophysics and Space Science Library*, Vol. 356, ed. M Gudipati, J Castillo-Rogez, pp. 409–54. New York: Springer

Choukroun M, Sotin C. 2012. Is Titan's shape caused by its meteorology and carbon cycle? *Geophys. Res. Lett.* 39:L04201

Cockell CS, Bush T, Bryce C, Direito S, Fox-Powell M, et al. 2016. Habitability: a review. *Astrobiology* 16(1):89–117

Connolly JAD. 1990. Multivariable phase diagrams—an algorithm based on generalized thermodynamics. *Am. J. Sci.* 290(6):666–718

Corlies P, Hayes AG, Birch SPD, Lorenz R, Stiles BW, et al. 2017. Titan's topography and shape at the end of the Cassini mission. *Geophys. Res. Lett.* 44(23):11754–61

Croft SK. 1982. A first-order estimate of shock heating and vaporization in oceanic impacts. In *Geological Implications of Impacts of Large Asteroids and Comets on Earth*, ed. TL Silver, PH Schultz, pp. 143–52. *Geol. Soc. Am. Spec. Pap.* 90. Boulder, CO: Geol. Soc. Am.

Croft SK, Lunine JI, Kargel J. 1988. Equation of state of ammonia-water liquid: derivation and planetological applications. *Icarus* 73(2):279–93

Durante D, Hemingway D, Racioppa P, Iess L, Stevenson D. 2019. Titan's gravity field and interior structure after Cassini. *Icarus* 326:123–32

Durham WB, Stern LA. 2001. Rheological properties of water ice—applications to satellites of the outer planets. *Annu. Rev. Earth Planet. Sci.* 29:295–330

Durham WB, Stern LA, Kirby SH. 1996. Rheology of water ices V and VI. *J. Geophys. Res.* 101(B2):2989–3001

Durham WB, Stern LA, Kirby SH. 1997. Creep of water ices at planetary conditions: a compilation. *J. Geophys. Res.* 102(E7):16293–302

Durham WB, Stern LA, Kirby SH. 2001. Rheology of ice I at low stress and elevated confining pressure. *J. Geophys. Res.* 106(B6):11031–42

Elachi C, Allison MD, Borgarelli L, Encrenaz P, Im E, et al. 2004. Radar: the Cassini Titan RADAR mapper. *Space Sci. Rev.* 115(1–4):71–110

Fischer G, Gurnett DA. 2011. The search for Titan lightning radio emissions. *Geophys. Res. Lett.* 38:L08206

Fortes AD. 2012. Titan's internal structure and the evolutionary consequences. *Planet. Space Sci.* 60(1):10–17

Fortes AD, Grindrod PM, Trickett SK, Vočadlo L. 2007. Ammonium sulfate on Titan: possible origin and role in cryovolcanism. *Icarus* 188(1):139–53

Friedson AJ, Stevenson DJ. 1983. Viscosity of rock-ice mixtures and applications to the evolution of icy satellites. *Icarus* 56(1):1–14

Fulchignoni M, Ferri F, Angrilli F, Ball AJ, Bar-Nun A, et al. 2005. In situ measurements of the physical characteristics of Titan's environment. *Nature* 438(7069):785–91

Gao P, Stevenson DJ. 2013. Nonhydrostatic effects and the determination of icy satellites' moment of inertia. *Icarus* 226(2):1185–91

Gastine T, Wicht W, Aubert J. 2016. Scaling regimes in spherical shell rotating convection. *J. Fluid Mech.* 808:690–732

Glein CR. 2015. Noble gases, nitrogen, and methane from the deep interior to the atmosphere of Titan. *Icarus* 250:570–86

Goldsby DL, Kohlstedt DL. 2001. Superplastic deformation of ice: experimental observations. *J. Geophys. Res.* 106(B6):11017–30

Grasset O, Pargamin J. 2005. The ammonia-water system at high pressures: implications for the methane of Titan. *Planet. Space Sci.* 53(4):371–84

Grasset O, Sotin C. 1996. The cooling rate of a liquid shell in Titan's interior. *Icarus* 123(1):101–12

Griffith C, Mitchell JL, Lavvas P, Tobie G. 2013. Titan's evolving climate. In *Comparative Climatology of Terrestrial Planets*, ed. SJ Mackwell, AA Simon-Miller, JW Harder, MA Bullock, R Dotson, pp. 91–119. Tucson: Univ. Ariz. Press

Griffith CA, Penteado PF, Rannou P, Brown R, Boudon V, et al. 2006. Evidence for a polar ethane cloud on Titan. *Science* 313(5793):1620–22

Griffith CA, Penteado PF, Turner JD, Neish CD, Mitri G, et al. 2019. A corridor of exposed ice-rich bedrock across Titan's tropical region. *Nat. Astron.* 3(7):642–48

Hay HCFC, Matsuyama I. 2017. Numerically modelling tidal dissipation with bottom drag in the oceans of Titan and Enceladus. *Icarus* 281:342–56

Hilairet N, Reynard B, Wang YB, Daniel I, Merkel S, et al. 2007. High-pressure creep of serpentine, interseismic deformation, and initiation of subduction. *Science* 318(5858):1910–13

Hogenboom DL, Kargel JS, Consolmagno GJ, Holden TC, Lee L, Buyyounouski M. 1997. The ammonia-water system and the chemical differentiation of icy satellites. *Icarus* 128(1):171–80

Hörst SM. 2017. Titan's atmosphere and climate. *J. Geophys. Res. Planets* 122(3):432–82

Hussmann H, Choblet G, Lainey V, Matson DL, Sotin C, et al. 2010. Implications of rotation, orbital states, energy sources, and heat transport for internal processes in icy satellites. *Space Sci. Rev.* 153(1–4):317–48

Iess L, Jacobson RA, Ducci M, Stevenson DJ, Lunine JI, et al. 2012. The tides of Titan. *Science* 337(6093):457–59

Iess L, Rappaport NJ, Jacobson RA, Racioppa P, Stevenson DJ, et al. 2010. Gravity field, shape, and moment of inertia of Titan. *Science* 327(5971):1367–69

Jaumann R, Brown RH, Stephan K, Barnes JW, Soderblom LA, et al. 2008. Fluvial erosion and post-erosional processes on Titan. *Icarus* 197(2):526–38

Journaux B, Brown JM, Pakhomova A, Collings IE, Petitgirard S, et al. 2020a. Holistic approach for studying planetary hydrospheres: Gibbs representation of ices thermodynamics, elasticity, and the water phase diagram to 2,300 MPa. *J. Geophys. Res. Planets* 125(1):e2019JE006176

Journaux B, Kalousová K, Sotin C, Tobie G, Vance S, et al. 2020b. Large ocean worlds with high-pressure ices. *Space Sci. Rev.* 216:7

Kalousová K, Sotin C. 2018. Melting in high-pressure ice layers of large ocean worlds—implications for volatiles transport. *Geophys. Res. Lett.* 45(16):8096–103

Kalousová K, Sotin C. 2020a. Dynamics of Titan's high-pressure ice layer. *Earth Planet. Sci. Lett.* 545:116416

Kalousová K, Sotin C. 2020b. The insulating effect of methane clathrate crust on Titan's thermal evolution. *Geophys. Res. Lett.* 47(13):e2020GL087481

Kalousová K, Sotin C, Choblet G, Tobie G, Grasset O. 2018. Two-phase convection in Ganymede's high-pressure ice layer—implications for its geological evolution. *Icarus* 299:133–47

Khurana KK, Kivelson MG, Stevenson DJ, Schubert G, Russell CT, et al. 1998. Induced magnetic fields as evidence for subsurface oceans in Europa and Callisto. *Nature* 395(6704):777–80

Kirk RL, Howington-Kraus E, Redding B, Aharonson O, Bills BG, et al. 2013. *Topographic mapping of Titan: completion of a global radargrammetric control network opens the floodgates for stereo DTM production*. Paper presented at the 44th Lunar and Planetary Science Conference, The Woodlands, Texas, Mar. 18–22

Kirk RL, Stevenson DJ. 1987. Thermal evolution of a differentiated Ganymede and implications for surface features. *Icarus* 69(1):91–134

Kivelson MG, Khurana KK, Russell CT, Walker RJ, Warnecke J, et al. 1996. Discovery of Ganymede's magnetic field by the Galileo spacecraft. *Nature* 384(6609):537–41

Kivelson MG, Khurana KK, Volwerk M. 2002. The permanent and inductive magnetic moments of Ganymede. *Icarus* 157(2):507–22

Kruijer TS, Burkhardt C, Budde G, Kleine T. 2017. Age of Jupiter inferred from the distinct genetics and formation times of meteorites. *PNAS* 114(26):6712–16

Kuramoto K, Matsui T. 1994. Formation of a hot proto-atmosphere on the accreting giant icy satellite: implications for the origin and evolution of Titan, Ganymede, and Callisto. *J. Geophys. Res.* 99(E10):21183–200

Kvorka J, Čadek O, Tobie G, Choblet G. 2018. Does Titan's long-wavelength topography contain information about subsurface ocean dynamics? *Icarus* 310:149–64

Lainey V, Casajus LG, Fuller J, Zannoni M, Tortora P, et al. 2020. Resonance locking in giant planets indicated by the rapid orbital expansion of Titan. *Nat. Astron.* 4:1053–58

Lavvas PP, Coustenis A, Vardavas IM. 2008. Coupling photochemistry with haze formation in Titan's atmosphere, Part II: results and validation with Cassini/Huygens data. *Planet. Space Sci.* 56(1):67–99

Le Mouélic S, Cornet T, Rodriguez S, Sotin C, Seignovert B, et al. 2019. The Cassini VIMS archive of Titan: from browse products to global infrared color maps. *Icarus* 319:121–32

Le Mouélic S, Paillou P, Janssen MA, Barnes JW, Rodriguez S, et al. 2008. Mapping and interpretation of Sinlap crater on Titan using Cassini VIMS and RADAR data. *J. Geophys. Res.* 113(E4):E04003

Lefevre A, Tobie G, Choblet G, Čadek O. 2014. Structure and dynamics of Titan's outer icy shell constrained from Cassini data. *Icarus* 237:16–28

Leitner MA, Lunine JI. 2019. Modeling early Titan's ocean composition. *Icarus* 333:61–70

Lopes RMC, Kirk RL, Mitchell KL, LeGall A, Barnes JW, et al. 2013. Cryovolcanism on Titan: new results from Cassini RADAR and VIMS. *J. Geophys. Res. Planets* 118:416–35

Lorenz RD, Le Gall A. 2020. Schumann resonance on Titan: a critical *Re*-assessment. *Icarus* 351:113942

Lorenz RD, Panning M, Staehler SC, Shiraishi H, Yamada R, Turtle EP. 2019. *Titan seismology with Dragonfly: probing the internal structure of the most accessible ocean world*. Paper presented at the 50th Lunar and Planetary Science Conference, The Woodlands, Texas, Mar. 18–22

Lorenz RD, Stiles BW, Kirk RL, Allison MD, del Marmo PP, et al. 2008. Titan's rotation reveals an internal ocean and changing zonal winds. *Science* 319(5870):1649–51

Loveday JS, Nelmes RJ, Guthrie M, Belmonte SA, Allan DR, et al. 2001. Stable methane hydrate above 2 GPa and the source of Titan's atmospheric methane. *Nature* 410:661–63

Lunine JI, Stevenson DJ. 1987. Clathrate and ammonia hydrates at high pressure: application to the origin of methane on Titan. *Icarus* 70(1):61–77

Marounina N, Grasset O, Tobie G, Carpy S. 2018. Role of the global water ocean on the evolution of Titan's primitive atmosphere. *Icarus* 310:127–39

Meriggiola R, Iess L. 2012. *A new rotational model of Titan from Cassini SAR data*. Paper presented at the European Planetary Science Congress 2012, Madrid, Spain, Sept. 23–28

Merrigiola R, Iess L, Stiles BW, Lunine JI, Mitri G. 2016. The rotational dynamics of Titan from Cassini RADAR images. *Icarus* 275:183–92

Miller KE, Glein CR, Waite JH Jr. 2019. Contributions from accreted organics to Titan's atmosphere: new insights from cometary and chondritic data. *Astrophys. J.* 871:59

Mitchell JL, Lora JM. 2016. The climate of Titan. *Annu. Rev. Earth Planet. Sci.* 44:353–80

Mitri G, Meriggiola R, Hayes A, Lefevre A, Tobie G, et al. 2014. Shape, topography, gravity anomalies and tidal deformation of Titan. *Icarus* 236:169–77

Mitri G, Showman AP, Lunine JI, Lopes RMC. 2008. Resurfacing of Titan by ammonia-water cryomagma. *Icarus* 196(1):216–24

Monteux J, Coltice N, Dubuffet F, Ricard Y. 2007. Thermo-mechanical adjustment after impacts during planetary growth. *Geophys. Res. Lett.* 34(24):L24201

Monteux J, Tobie G, Choblet G, Le Feuvre M. 2014. Can large icy moons accrete undifferentiated? *Icarus* 237:377–87

Mueller S, McKinnon WB. 1988. Three-layered models of Ganymede and Callisto: compositions, structures, and aspects of evolution. *Icarus* 76(3):437–64

Murshed MM, Schmidt BC, Kuhs WF. 2010. Kinetics of methane-ethane gas replacement in clathrate-hydrates studied by time-resolved neutron diffraction and Raman spectroscopy. *J. Phys. Chem. A* 114:247–55

Nagel K, Breuer D, Spohn T. 2004. A model for the interior structure, evolution, and differentiation of Callisto. *Icarus* 169(2):402–12

Neish CD, Lorenz RD. 2012. Titan's global crater population: a new assessment. *Planet. Space Sci.* 60:26–33

Néri A, Guyot F, Reynard B, Sotin C. 2020. A carbonaceous chondrite and cometary origin for icy moons of Jupiter and Saturn. *Earth Planet. Sci. Lett.* 530:115920

Niemann HB, Atreya SK, Bauer SJ, Carignan GR, Demick JE, et al. 2005. The abundances of constituents of Titan's atmosphere from the GCMS instrument on the Huygens probe. *Nature* 438(7069):779–84

Niemann HB, Atreya SK, Demick JE, Gautier D, Haberman JA, et al. 2010. Composition of Titan's lower atmosphere and simple surface volatiles as measured by the Cassini-Huygens probe gas chromatograph mass spectrometer experiment. *J. Geophys. Res.* 115(E12):E12006

Nimmo F, Bills BG. 2010. Shell thickness variations and the long-wavelength topography of Titan. *Icarus* 208(2):896–904

O'Rourke JG, Stevenson DJ. 2014. Stability of ice/rock mixtures with application to a partially differentiated Titan. *Icarus* 227:67–77

Rekier J, Trinh A, Triana SA, Dehant V. 2019. Internal energy dissipation in Enceladus's subsurface ocean from tides and libration and the role of inertial waves. *J. Geophys. Res. Planets* 124(8):2198–212

Rovira-Navarro M, Rieutord M, Gerkema T, Maas LRM, van der Wal W, Vermeersen B. 2019. Do tidally-generated inertial waves heat the subsurface oceans of Europa and Enceladus? *Icarus* 321:126–40

Sagan C, Dermott SF. 1982. The tide in the seas of Titan. *Nature* 300(5894):731–33

Sasaki T, Stewart GR, Ida S. 2010. Origin of the different architectures of the Jovian and Saturnian satellite systems. *Astrophys. J.* 714(2):1052–64

Saur J, Neubauer FM, Glassmeier KH. 2010. Induced magnetic fields in solar system bodies. *Space Sci. Rev.* 152(1–4):391–421

Sears WD. 1995. Tidal dissipation in oceans on Titan. *Icarus* 113(1):39–56

Senshu H, Kuramoto K, Matsui T. 2002. Thermal evolution of a growing Mars. *J. Geophys. Res.* 107(E12):5118
Showman AP, Malhotra R. 1999. The Galilean satellites. *Science* 286(5437):77–84
Simoes F, Grard R, Hamelin M, Lopez-Morenoc JJ, Schwingenschuh K, et al. 2007. A new numerical model for the simulation of ELF wave propagation and the computation of eigenmodes in the atmosphere of Titan: Did Huygens observe any Schumann resonance? *Planet. Space Sci.* 55(13):1978–89
Sloan E, Koh CA. 2007. *Clathrate Hydrates of Natural Gases*. Boca Raton, FL: CRC
Soderlund KM. 2019. Ocean dynamics of outer solar system satellites. *Geophys. Res. Lett.* 46(15):8700–10
Soderlund KM, Kalousová K, Buffo JJ, Glein CR, Goodman JC, et al. 2020. Ice-ocean exchange processes in the Jovian and Saturnian satellites. *Space Sci. Rev.* 216:80
Sohl F, Sears WD, Lorenz RD. 1995. Tidal dissipation on Titan. *Icarus* 115(2):278–94
Sohl F, Spohn T, Breuer D, Nagel K. 2002. Implications from Galileo observations on the interior structure and chemistry of the Galilean satellites. *Icarus* 157(1):104–19
Sotin C, Gillet P, Poirier J-P. 1985. Creep of high-pressure ice VI. In *Ices in the Solar System*, ed. J Klinger, D Benest, A Dollfus, R Smoluchowski, pp. 109–18. Dordrecht, Neth.: Reidel
Sotin C, Poirier J-P. 1987. Viscosity of ice V. *J. Phys. Colloq.* 48(C1):233–38
Stiles BW, Kirk RL, Lorenz RD, Hensley S, Lee E, et al. 2008. Determining Titan's spin state from Cassini radar images. *Astron. J.* 135(5):1669–80. Erratum. 2010. *Astron. J.* 139(1):311
Stofan ER, Elachi C, Lunine JI, Lorenz RD, Stiles B, et al. 2007. The lakes of Titan. *Nature* 445:61–64
Tobie G, Choukroun M, Grasset O, Le Mouélic S, Lunine JI, et al. 2009. Evolution of Titan and implications for its hydrocarbon cycle. *Philos. Trans. R. Soc. A* 367(1889):617–31
Tobie G, Gautier D, Hersant F. 2012. Titan's bulk composition constrained by Cassini-Huygens: implication for internal outgassing. *Astrophys. J.* 752(2):125
Tobie G, Grasset O, Lunine JI, Mocquet A, Sotin C. 2005a. Titan's internal structure inferred from a coupled thermal-orbital model. *Icarus* 175(2):496–502
Tobie G, Lunine J, Monteux J, Mousis O, Nimmo F. 2014. The origin and evolution of Titan. In *Titan: Interior, Surface, Atmosphere, and Space Environment*, ed. I Müller-Wodarg, C Griffith, E Lellouch, T Cravens, pp. 29–62. Cambridge, UK: Cambridge Univ. Press
Tobie G, Lunine JI, Sotin C. 2006. Episodic outgassing as the origin of atmospheric methane on Titan. *Nature* 440:61–64
Tobie G, Mocquet A, Sotin C. 2005b. Tidal dissipation within large icy satellites: applications to Europa and Titan. *Icarus* 177(2):534–49
Tomasko MG, Archinal B, Becker T, Bézard B., Bushroe M, et al. 2005. Rain, winds and haze during the Huygens probe's descent to Titan's surface. *Nature* 438(7069):765–78
Turtle EP, Barnes JW, Trainer MG, Lorenz RD, MacKenzie SM, et al. 2017. *Dragonfly: exploring Titan's prebiotic organic chemistry and habitability*. Paper presented at the 48th Lunar and Planetary Science Conference, The Woodlands, Texas, Mar. 20–24
Tyler RH. 2008. Strong ocean tidal flow and heating on moons of the outer planets. *Nature* 456(7223):770–72
Vance SD, Bouffard M, Choukroun M, Sotin C. 2014. Ganymede's internal structure including thermodynamics of magnesium sulfate oceans in contact with ice. *Planet. Space Sci.* 96:62–70
Vance SD, Brown JM. 2013. Thermodynamic properties of aqueous $MgSO_4$ to 800 MPa at temperatures from −20 to 100°C and concentrations to 2.5 mol kg^{-1} from sound speeds, with applications to icy world oceans. *Geochim. Cosmochim. Acta* 110:176–89
Vance SD, Panning MP, Stahler S, Cammarano F, Bills BG, et al. 2018. Geophysical investigations of habitability in ice-covered ocean worlds. *J. Geophys. Res. Planets* 123(1):180–205
Van Hoolst T, Baland R-M, Trinh A. 2013. On the librations and tides of large icy satellites. *Icarus* 226(1):299–315
Van Hoolst T, Rambaux N, Karatekin O, Baland R-M. 2009. The effect of gravitational and pressure torques on Titan's length-of-day variations. *Icarus* 200(1):256–64
Vu TH, Choukroun M, Sotin C, Muñoz-Iglesias V, Maynard-Casely HE. 2020. Rapid formation of clathrate hydrate from liquid ethane and water ice on Titan. *Geophys. Res. Lett.* 47:e2019GL086265
Wagner W, Riethmann T, Feistel R, Harvey AH. 2011. New equations for the sublimation pressure and melting pressure of H_2O ice Ih. *J. Phys. Chem. Ref. Data* 40(4):043103

Wagner W, Saul A, Pruss A. 1994. International equations for the pressure along the melting and along the sublimation curve of ordinary water substance. *J. Phys. Chem. Ref. Data* 23(3):515–27

Wasson JT, Kallemeyn GW. 1988. Composition of chondrites. *Philos. Trans. R. Soc. A* 325(1587):535–44

Werynski A, Neish C, Gall AL, Janssen M. 2019. Compositional variations of Titan's impact craters indicates active surface erosion. *Icarus* 321:508–21

Yung YL, Allen M, Pinto JP. 1984. Photochemistry of the atmosphere of Titan: comparison between model and observations. *Astrophys. J. Suppl. Ser.* 55:465–506

Zahnle KJ, Korycansky DG, Nixon CA. 2014. Transient climate effects of large impacts on Titan. *Icarus* 229:378–91

Zebker HA, Gim Y, Callahan P, Hensley S, Lorenz R, Team Cassini Radar. 2009. Analysis and interpretation of Cassini Titan radar altimeter echoes. *Icarus* 200(1):240–55